Contents

Chapter 1

Finite Difference Methods for Turbulence Simulations

Aditya Ghate[a] and Sanjiva K. Lele[b,c]

[a]Science & Technology Corporation, NASA Ames Research Center, [b]Department of Aeronautics and Astronautics, Stanford University, [c]Department of Mechanical Engineering, Stanford University

1.1 INTRODUCTION

The optimal finite difference discretization used in simulations of turbulent flows is influenced by both, the type of the scale resolving simulation (DNS or LES), as well as the flow-physics (hydrodynamic instabilities, shocks, acoustics, etc.) one expects to resolve. Insight into dispersion and dissipation error requirements for some common scale-resolving simulation scenarios help to highlight the issues faced in selecting a scheme.

1. **Fully Resolved Numerical Simulation (FRNS) of turbulence**: Schemes with *low dispersion* errors and *zero dissipation* errors are the most attractive for such flows. Since the intention is to resolve all physical dissipation (which peaks close to walls, within shock waves, and at high-wavenumbers) while minimizing computational cost, schemes such as Pade finite differences[2] and optimized explicit finite difference (such as dispersion relation preserving) schemes[1] can be very promising as they offer spectral-like accuracy at substantially higher grid, domain and boundary condition flexibility. Robustness of these discretizations can be achieved using reduced aliasing formulations discussed in Section 1.4.1.
2. **Direct Numerical Simulation (DNS) of turbulence with shock and/or interface capturing**: Schemes with *low dispersion* errors and *spatially localized dissipation* errors are preferable due to their shock capturing capabilities. Non-linear schemes[1] such as Weighted Essentially Non-Oscillatory (WENO)[4] and Weighted Compact Non-linear Schemes (WCNS)[3] that possess superior monotonicity preserving properties compared to linear central schemes have been very successful in DNS of turbulence involving shocks and multi-material interfaces. These schemes are also popular for under-resolved direct simulations (sometimes referred to as implicit LES) of mul-

1. schemes where stencil weights are functions of the local flow variables

tiphysics problems (such as variable-density and/or multiphase turbulence) where physics-informed subgrid scale closure models are lacking. Section 1.4.2.1 focuses on such hybrid schemes. Numerical/artificial fluid properties for bulk viscosity and thermal diffusivity (see Section 1.4.2.2) based on high-wavenumber biased kernels for localization are effective at regularizing weak shocks and material interfaces with (numerical) thickness substantially smaller than the dissipation (solenoidal/vortical) length scales that are desired to be resolved by the DNS. The effectiveness of turbulence resolving, but shock-capturing direct simulations (using an appropriate monotonicity preserving discretization) was recently studied by Tian et al.[179] on a canonical shock-turbulence interaction problem. The authors were able to demonstrate that both the streamwise and spanwise components of the Reynolds stress resolved in their turbulence-resolving-but-shock-capturing simulations approached the limits predicted by Linear Interaction Approximation (LIA) on coarser grids compared to shock-resolving direct simulations.

3. **Large Eddy Simulations (LES) of turbulence with or without shocks and/or material interfaces**: As discussed in Chapter 1, at high Reynolds numbers only low-pass filtered solutions of Navier-Stokes equations, designed to resolve turbulent kinetic energy (based on an appropriately defined L2 norm) are computationally tractable. The vast majority of Large Eddy Simulations performed for high-Reynolds number turbulence are characterized by a spatial filtering length scale corresponding to the Nyquist resolution of the computational grid being utilized. Subgrid scale-closure models designed to accurately capture statistical spatio-temporal characteristics of energy transfer between resolvable and subgrid scales of motion, invariably carry $O(1)$ local errors. The accuracy of LES is typically far more sensitive to dissipative properties of the numerical discretization as opposed to its dispersion properties. While this is primarily true for flows lacking mean convection, many LES applications do involve mean convection and in such cases dispersion errors of numerical schemes do matter. For LES Linear Schemes with low operational complexity (including second order accurate) discretizations offer very attractive cost/accuracy properties including discrete kinetic energy and entropy preservation. For problems involving shock and/or material discontinuities, physics based sensors need to be used to blend schemes having shock-capturing properties with central schemes to achieve a pragmatic compromise for the numerical dissipation needed to prevent Gibbs-oscillations at solution discontinuities while preventing scheme-dissipation in vorticity-dominated regions. Section 1.7 focuses on use of finite difference discretizations for LES.
4. **Large Eddy Simulations (LES) with dominant linear dynamics (acoustics, wave propagation, and instabilities)** : Schemes with *low dispersion errors* and *controlled dissipation* properties to minimize dispersion errors up to a certain points-per-wavelength (`ppw`) criterion and to dissipate/dampen errors beyond the desired `ppw` (*small spatial scales*) are desirable for resolving

long range wave propagation (acoustics, instability waves). While selective filtering[5] can be used to accomplish this, schemes with low dispersion errors and controlled dissipation can also improve non-linear robustness which is desirable for LES of high-Reynolds number flows. Section 1.5 addresses this type of discretization.

1.2 GRID TOPOLOGIES

The single most-influential attribute of any scale resolving turbulence simulation is the grid system. Two topologically distinct grid systems: a) Curvilinear overset and/or multiblock, and b) Cartesian octree, are commonly used in finite difference formulations and can address a variety of complex flows including large disparate scales of motions as well as complex geometries. Figure 1.1 shows both curvilinear and Cartesian grid systems deployed for LES of a full aircraft configuration (High Lift Common Research Model) to investigate the highly complex flow physics.

1.2.1 Navier Stokes Equations in Curvilinear Coordinates

Conservation laws such as the Navier-Stokes equations expressed in curvilinear coordinates provide a powerful foundation for utilization of finite difference methods (of arbitrarily high order) on problems involving non-trivial geometries and domains. This chapter develops the curvilinear formulation using an analytic *wavy mesh* shown in Figure 1.2[6] as an example. Consider a general boundary-conforming invertible non-stationary (moving) transformation of governing equations to curvilinear coordinates[7] in 2-dimensions[2].

$$\xi = \xi(x, y, t) \;\; , \;\; \eta = \eta(x, y, t) \;\; , \tau = t \tag{1.1}$$

with its inverse map

$$x = x(\xi, \eta, \tau) \;\; , \;\; y = y(\xi, \eta, \tau) \;\; , \;\; t = \tau \tag{1.2}$$

The basic principle of the transformation is to map an arbitrary curvilinear structured grid to a uniform Cartesian grid in the *computational space*. Chain-rule allows computation of derivatives on the physical grid using finite difference operators implemented in computational space:

$$\begin{bmatrix} \partial_x \\ \partial_y \\ \partial_t \end{bmatrix} = \underbrace{\begin{bmatrix} \xi_x & \eta_x & 0 \\ \xi_y & \eta_y & 0 \\ \xi_t & \eta_t & 1 \end{bmatrix}}_{\boldsymbol{T}^{-1}} \begin{bmatrix} \partial_\xi \\ \partial_\eta \\ \partial_\tau \end{bmatrix} \qquad \text{and} \qquad \begin{bmatrix} \partial_\xi \\ \partial_\eta \\ \partial_\tau \end{bmatrix} = \underbrace{\begin{bmatrix} x_\xi & y_\xi & 0 \\ x_\eta & y_\eta & 0 \\ x_\tau & y_\tau & 1 \end{bmatrix}}_{\boldsymbol{T}} \begin{bmatrix} \partial_x \\ \partial_y \\ \partial_t \end{bmatrix} \tag{1.3}$$

2. The two dimensional case is considered here for simplicity, and an extension to the full three-dimensional case is straightforward.

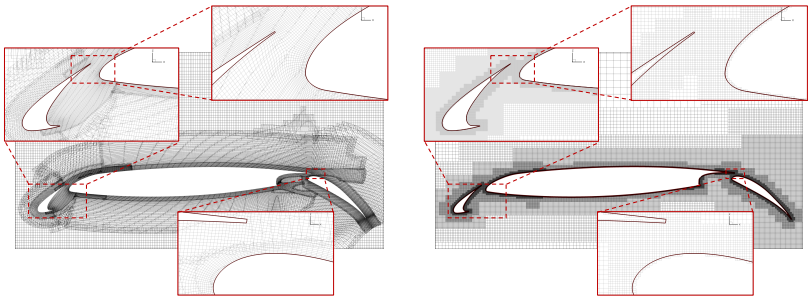

(a) Curvilinear Overset (b) Cartesian Octree

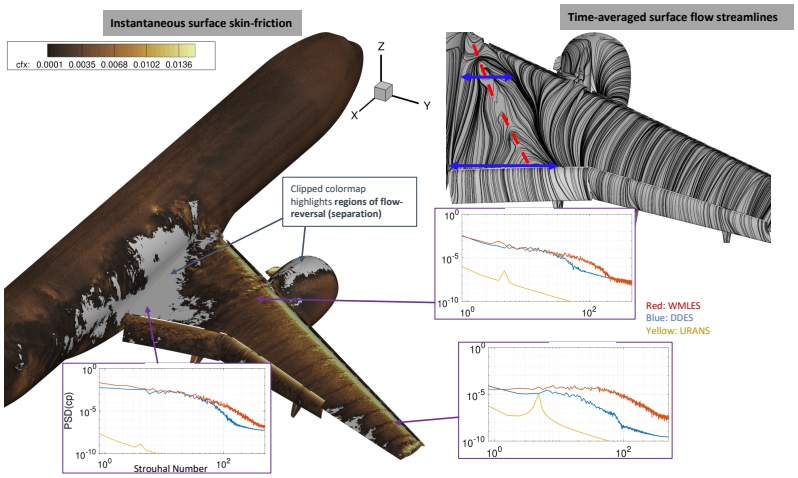

(c) Wall Modelled LES of High-Lift CRM at angle of attack, $\alpha = 21.47°$ depicting the onset of inboard stall along with comparisons of the unsteady pressure fluctuations captured by two scale-resolving methods: WMLES and DDES with URANS. Numerical schemes for URANS or RANS are not discussed in this chapter.

FIGURE 1.1 Two distinct mesh topologies used for Wall-modelled Large Eddy Simulations (WMLES) of the High-Lift Common Research Model (HL-CRM). Both mesh topologies allow for higher order accurate finite difference discretizations; a 4th order inviscid flux discretization and a second order viscous flux discretization were utilized in the simulations. While the curvilinear, body-aligned overset grid system allows for very detailed grid tailoring (grid aspect ratio, wake refinement, etc.), it requires substantial human effort for generation, and can take months to complete. In contrast, the Cartesian Octree meshing allows automation and can be generated in a few seconds. However, since the Cartesian grids are not body-aligned, the geometry representation requires robust and highly accurate immersed boundary representation of the geometry. The reader is referred to Kiris et al.[78] and Ghate et al.[79] for detailed discussions and analysis of the simulations performed. Image credit: Gerrit-Daniel Stich (Curvilinear grid), Gaetan Kenway (Cartesian Octree grid) and Oliver Browne (Time-averaged Streamlines) from NASA Ames Research Center.

The invertibility property of the transformation matrix $\left(\boldsymbol{T^{-1}}\right)^{-1} = \boldsymbol{T}$ results in several useful identities:

$$x_\xi = J_T \eta_y \ , \ y_\xi = -J_T \eta_x \ , \ x_\eta = -J_T \xi_y \ , \ y_\eta = J_T \xi_x \tag{1.4}$$

$$\xi_x = J_T^{-1} y_\eta \ , \ \eta_x = -J_T^{-1} y_\xi \ , \ \xi_y = -J_T^{-1} x_\eta \ , \ \eta_y = J_T^{-1} x_\xi \tag{1.5}$$

and

$$x_\tau = J_T \left(\xi_y \eta_t - \eta_y \xi_t\right) \ , \ y_\tau = J_T \left(\eta_x \xi_t - \xi_x \eta_t\right) \tag{1.6}$$

$$\xi_t = J_T^{-1} \left(x_\eta y_\tau - y_\eta x_\tau\right) \ , \ \eta_t = J_T^{-1} \left(x_\tau y_\xi - y_\tau x_\xi\right) \tag{1.7}$$

where the scalar term, $J_T = x_\xi y_\eta - x_\eta y_\xi$ is the determinant of the transformation matrix $\boldsymbol{T}$, and is often referred to as the Jacobian of the map or the metric volume term since it represents the local cell volume (cell area in two dimensions).

1.2.1.1 Conservation laws on curvilinear grids

Consider a generic conservation law for a vector field, $\boldsymbol{U}$ in two dimensions

$$\boldsymbol{U}_t + \boldsymbol{F}_x + \boldsymbol{G}_y = 0 \tag{1.8}$$

where $\boldsymbol{F}$ and $\boldsymbol{G}$ are the corresponding vector fluxes in x and y respectively. Using chain rule, we can simplify the conservation law above as follows

$$\boldsymbol{U}_\tau + \xi_t \boldsymbol{U}_\xi + \eta_t \boldsymbol{U}_\eta + \xi_x \boldsymbol{F}_\xi + \eta_x \boldsymbol{F}_\eta + \xi_y \boldsymbol{G}_\xi + \eta_y \boldsymbol{G}_\eta = 0 \tag{1.9}$$

Multiplying the above equation by the Jacobian, J_T and using the metric identities stated in Equation 1.4 - 1.7, we get the following *transformed* conservation law

$$\tilde{\boldsymbol{U}}_\tau + \tilde{\boldsymbol{F}}_\xi + \tilde{\boldsymbol{G}}_\eta = 0 \tag{1.10}$$

where

$$\tilde{\boldsymbol{U}} = J_T \boldsymbol{U} \ , \ \tilde{\boldsymbol{F}} = J_T \left(\boldsymbol{F}\xi_x + \boldsymbol{G}\xi_y + \boldsymbol{U}\xi_t\right) \ , \ \tilde{\boldsymbol{G}} = J_T \left(\boldsymbol{F}\eta_x + \boldsymbol{G}\eta_y + \boldsymbol{U}\eta_t\right) \tag{1.11}$$

To understand the conservation law in the transformed computational coordinates, consider the following simplification of transformed flux $\tilde{\boldsymbol{F}}$:

$$\tilde{\boldsymbol{F}} = J_T \left(\boldsymbol{F}\xi_x + \boldsymbol{G}\xi_y + \boldsymbol{U}\xi_t\right) = \boldsymbol{F} y_\eta - \boldsymbol{G} x_\eta + \boldsymbol{U} \left(x_\eta y_\tau - y_\eta x_\tau\right) \tag{1.12}$$

Here the term $\boldsymbol{F} y_\eta - \boldsymbol{G} x_\eta$ represents the vector rotation of the Cartesian fluxes $\boldsymbol{F}$ and $\boldsymbol{G}$ from (x, y) coordinates to the new (ξ, η) coordinates. The last term containing $\left(x_\eta y_\tau - y_\eta x_\tau\right)$ corresponds to the movement of the (ξ, η, τ) coordinate system in the (x, y, t) coordinate system. Flux $\tilde{\boldsymbol{F}}$ is orthogonal to a line of constant η while $\tilde{\boldsymbol{G}}$ is orthogonal to a line of constant ξ. The curvilinear fluxes, $\tilde{\boldsymbol{F}}$ and $\tilde{\boldsymbol{G}}$ are in ξ and η directions respectively, if and only if the transformed coordinate system (ξ, η, τ) is orthogonal - no such constraint is imposed by the general transformation introduced in Equation 1.3.

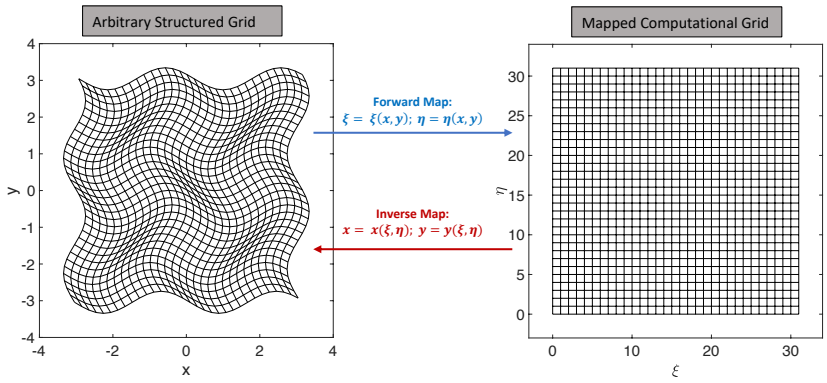

FIGURE 1.2 Illustration of a *stationary* curvilinear transform from *physical space* to *computational space* in 2D.

1.2.1.2 The geometric conservation constraint

Consider the curvilinear transformed three-dimensional Euler equation (zero viscosity limit of Navier-Stokes)

$$\tilde{\boldsymbol{Q}}_\tau + \tilde{\boldsymbol{E}}_\xi + \tilde{\boldsymbol{F}}_\eta + \tilde{\boldsymbol{G}}_\zeta = 0 \tag{1.13}$$

where

$$\boldsymbol{Q} = [\rho, \rho u, \rho v, \rho w, e] \tag{1.14}$$

$$\boldsymbol{E} = \left[\rho u, \rho u^2 + p, \rho uv, \rho uw, u(e+p)\right] \tag{1.15}$$

$$\boldsymbol{F} = \left[\rho v, \rho uv, \rho v^2 + p, \rho vw, v(e+p)\right] \tag{1.16}$$

$$\boldsymbol{G} = \left[\rho w, \rho uw, \rho vw, \rho w^2 + p, w(e+p)\right] \tag{1.17}$$

with the transformed variables given by

$$\tilde{\boldsymbol{Q}} = J_T \boldsymbol{Q} \tag{1.18}$$

$$\tilde{\boldsymbol{E}} = \hat{\xi}_t \boldsymbol{Q} + \hat{\xi}_x \boldsymbol{E} + \hat{\xi}_y \boldsymbol{F} + \hat{\xi}_z \boldsymbol{G} \tag{1.19}$$

$$\tilde{\boldsymbol{F}} = \hat{\eta}_t \boldsymbol{Q} + \hat{\eta}_x \boldsymbol{E} + \hat{\eta}_y \boldsymbol{F} + \hat{\eta}_z \boldsymbol{G} \tag{1.20}$$

$$\tilde{\boldsymbol{G}} = \hat{\zeta}_t \boldsymbol{Q} + \hat{\zeta}_x \boldsymbol{E} + \hat{\zeta}_y \boldsymbol{F} + \hat{\zeta}_z \boldsymbol{G} \tag{1.21}$$

$$\tag{1.22}$$

where $\hat{\xi}_x = J_T \xi_x, \hat{\eta}_x = J_T \eta_x$, etc. and J_T is the Jacobian or the metric volume term introduced earlier, but in three-dimensional coordinates. By splitting the time derivative term in Equation 1.13 as: $\tilde{\boldsymbol{Q}}_\tau = J_T \boldsymbol{Q}_\tau + (J_T)_\tau \boldsymbol{Q}$, Equation 1.13 simplifies to:

$$\boldsymbol{Q}_\tau = -\frac{1}{J_T}\left(\tilde{\boldsymbol{E}}_\xi + \tilde{\boldsymbol{F}}_\eta + \tilde{\boldsymbol{G}}_\zeta + (J_T)_\tau \boldsymbol{Q}\right) \tag{1.23}$$

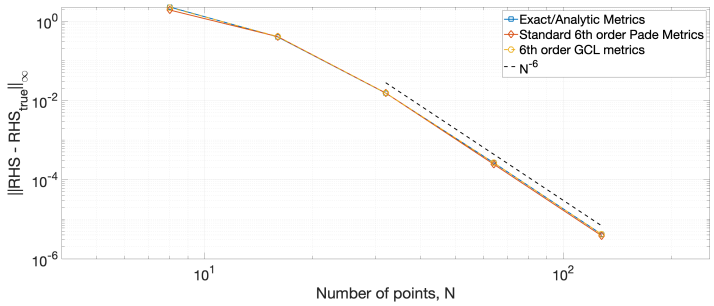

FIGURE 1.3 Error convergence (compressible Navier-Stokes with periodic BCs) evaluated using the method of manufactured solution on a 3D wavy mesh using 6th order Pade discretization. Three different methods are used to evaluate the metric terms.

Now, for a uniform free-stream (all field variables constant in space), Equation 1.23 can be written as:

$$\boldsymbol{Q}_\tau = -\frac{1}{J_T}\left(I_x\boldsymbol{E} + I_y\boldsymbol{F} + I_z\boldsymbol{G} + I_t\boldsymbol{Q}\right) \tag{1.24}$$

where

$$I_x = \left(\hat{\xi}_x\right)_\xi + \left(\hat{\eta}_x\right)_\eta + \left(\hat{\zeta}_x\right)_\zeta \tag{1.25}$$

$$I_y = \left(\hat{\xi}_y\right)_\xi + \left(\hat{\eta}_y\right)_\eta + \left(\hat{\zeta}_y\right)_\zeta \tag{1.26}$$

$$I_z = \left(\hat{\xi}_z\right)_\xi + \left(\hat{\eta}_z\right)_\eta + \left(\hat{\zeta}_z\right)_\zeta \tag{1.27}$$

$$I_t = \left(\hat{\xi}_t\right)_\xi + \left(\hat{\eta}_t\right)_\eta + \left(\hat{\zeta}_t\right)_\zeta + \left(J_T\right)_\tau \tag{1.28}$$

For discrete preservation of arbitrarily valued free-stream conditions, the finite difference scheme must satisfy $I_x = I_y = I_z = I_t = 0$. Here, $I_x = I_y = I_z = 0$ represents a differential statement for *surface conservation* while $I_t = 0$ represents the differential statement for *volume conservation*. Union of the two statements is often termed as the *Geometric Conservation Law* (GCL).

The standard definition of the metrics, $\hat{\xi}_x, \hat{\eta}_x, \hat{\zeta}_x$, etc. given as

$$\hat{\xi}_x = y_\eta z_\zeta - y_\zeta z_\eta \;\;,\;\; \hat{\eta}_x = y_\zeta z_\xi - y_\xi z_\zeta \;\;,\;\; \hat{\zeta}_x = y_\xi z_\eta - y_\eta z_\xi \;\;, \text{etc.} \tag{1.29}$$

when computed using standard finite difference schemes (including second order accurate schemes) violates the GCL conditions. When using non-dissipative discretizations (such as those needed in LES) these GCL errors contaminate the true solution at wavenumbers corresponding to grid non-uniformities. Pulliam & Steger[8] proposed solutions involving special 2nd order weighted averaging, as well as explicit removal of the free-stream fluxes from local fluxes. Both approaches achieved discrete GCL properties; however, a more elegant solution proposed by Thomas & Lombard[9], initially proposed for second order accurate

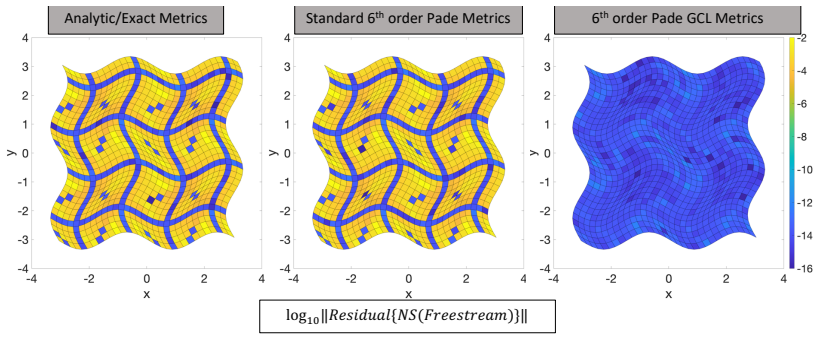

FIGURE 1.4 Residual error for a free-stream initial condition on a wavy mesh using three different metric evaluations.

formulation, later became more popular due to its flexibility in extensions for higher order discretizations. In this approach the metric terms are computed in a *conservative* manner by using modified definitions:

$$\hat{\xi}_x = (y_\eta z)_\zeta - (y_\zeta z)_\eta \ , \ \hat{\eta}_x = (y_\zeta z)_\xi - (y_\xi z)_\zeta \ , \ \hat{\zeta}_x = (y_\xi z)_\eta - (y_\eta z)_\xi \quad (1.30)$$

This approach has been successfully used and extended for a variety of finite difference discretizations including collocated Pade operators[6], non-linear (WENO/WCNS) and linear mid-point operators[10], and staggered/mid-point Pade operators[11]. Figure 1.3 shows the grid convergence obtained for a Navier-Stokes discretization on a 3D periodic wavy mesh using 6th order accurate Pade discretization. Three different methods are used for metric term evaluations, and the convergence plot shows essentially identical errors obtained in each of the three methods. However, when the same mesh is used for free-stream residual evaluation (see Figure 1.4), the two non-GCL preserving methods show large residual errors, while the GCL-preserving formulation shows errors corresponding to double-precision machine round-off.

When applied on stretched grids, central schemes (both implicit and explicit schemes) have dissipative character as well as the expected dispersion errors. A substantial body of work exists on the subject of error analysis on non-uniform and skewed grids[13–15]. Fourier-analysis applied to stretched grids show the limited benefits of high-order discretizations especially when grid stretching ratios exceed 10%. Optimized explicit finite difference schemes (such as DRP schemes) have been shown to provide better spectral properties at stretching ratios of 2% over equivalent traditional stencils; however no measurable benefits are obtained at stretching ratios of 8%[5]. Hence, when generating grids for LES or DNS, careful control over grid-stretching is needed as most of the LES studies for both shear-layer and wall-bounded turbulence utilize grid stretching ratios of under 10% in regions of the domain where resolving turbulent scales is desirable to limit dissipative numerical errors.

1.2.2 Cartesian Octree topologies

Finite difference schemes when used with Cartesian octree grids have several strengths over the curvilinear formulation discussed in the prior section which has led to their popular appeal in a variety of disciplines beyond turbulence, including cosmological hydrodynamics[16] and magnetohydrodynamics (MHD)[17]. Among these advantages are the automated grid generation[18] and adaptive mesh refinement (AMR)[19]. Much of the discussion of numerical schemes for the inviscid flux presented in Section 1.4 is focused on Cartesian formulation, and as such only certain salient aspects of Cartesian octree grids are emphasized in this section. Here we refer to Octree grids as a root Cartesian grid over the entire computational domain with sequence of hierarchical nested grid patches. Note that while the word *octree* suggests a 1-dimensional refinement ratio of 2:1 between successive levels (*quadtree* in two dimensions), majority of the algorithms can be extended to higher refinement ratios. Integer ratios between grid levels allow for non-uniform time integration such that the ratio Δ_x/Δ_t between grid levels l and $l+1$ is always constant. This can be particularly advantageous when feature-based refinement is used so that only a small subset of the total degrees-of-freedom requires the use of small time-step size which is typically limited by linear stability properties of the time integration scheme. The multi resolution property of the octree-grid topology makes it very attractive for grid adaptation in problems involving non-stationary turbulence (moving geometries, shocks, etc.) and many error indicators have been developed in the literature ranging from simple gradient detectors[107] to advanced wavelets[21,158].

1. **Coarse-fine interfaces.** A key distinction between Cartesian grids that use block-structured AMR with those that use forest-of-octrees is that in the former, a fine grid at level l always *covers* a coarser grid at level $l-1$. As such the finer grid patches are time integrated using Dirichlet boundary conditions via ghost cells which use interpolated values from level $l-1$. The cells on the coarse level, $l-1$ that are covered by the fine-grid cells at level l are over-written via a *restriction* operation on the fine grid. In the forest-of-octrees approach, both the coarse-level, $l-1$ and the fine level l are treated as independent domains using Dirichlet boundary conditions with the ghost cells filled via a spatio-temporal interpolation from the adjacent grid. Both approaches allow the use of high-order discretizations with the number of ghost cells dictated by the discretization stencil. For hyperbolic conservation laws using cell-centered formulations, the coarse-fine interface is defined via a common-midpoint between levels l and $l-1$. An additional flux-correction (or *refluxing*) step[19] can be used on such grids for discrete conservation, typically defined as a second order mid-point flux quadrature. The basic principle of this flux correction is to utilize the flux from the fine level grid, l for the common-midpoint shared by the levels l and $l-1$. In practice, since the coarse-level solution is time-advanced prior to the fine level solution, the coarse-grid solution at the cells adjacent to the finer level needs to be

corrected using the common-midpoint flux. For higher-order discretization stencils, the flux difference form[20] (discussed in Section 1.4) is utilized although the second order-quadrature results in second order accuracy at the solution points adjacent to the coarse-fine interface. Since coarse-fine interfaces correspond to mesh discontinuity (interpreted as filter-scale discontinuity in LES), additional stability promoting numerical treatment is often required when central/non-dissipative finite difference discretizations are used. Flux blending with non-linear schemes (such as WENO) near the coarse-fine interfaces has been used successfully in the past to prevent numerical instabilities[22].

2. **Linear Solvers.** In fluid mechanics simulations involving elliptic operators (incompressible, low-Mach variable density, MHD, implicit time-stepping, etc.) the linear solver typically dominates the complexity of the overall algorithm. Cartesian octree grids that are naturally suited for geometric multigrid based preconditioning have an advantage here over curvilinear finite difference or unstructured finite volume formulations. The reader is referred to the work by McCormick & Thomas[24] on *Fast Adaptive Composite* multigrid algorithms as well as that by Almgren et al.[23] on projection methods based on staggered variable storage for variable coefficient Poisson solver. The later work further details the modifications to composite multigrid V-cycles to account for the refluxing operation at coarse-fine interfaces.

1.2.3 Numerical considerations for abrupt grid changes

Both topologies discussed above suffer from a common numerical challenge - discretization robustness at regions of abrupt resolution changes. For the octree-grids, this can be seen as a factor of 8 abrupt change in cell volumes at coarse-fine interfaces, while for curvilinear overset grids, the overset locations can result in an arbitrary change in cell volume depending on the specific mesh design. The numerical artifacts associated with wave-propagation across such grid interfaces has been studied rigorously by Vichnevetsky [148,149], and more recently by Bhaksaran[175], Berland et al.[173] and Yalla et al.[150] in the context of LES. Tam & Hu[174] have studied the reflection issue in the context of curvilinear overset grids and proposed interpolation schemes that minmize acoustic reflections at interfaces. Chapter 1 explores this topic further via a linear advection example using two different wave-packets. Central finite difference discretizations have typically relied on selective filtering [6,126,138] near coarse-fine interfaces to address numerical stability issues and to dampen any reflected waves (especially acoustic waves). Blended schemes with upwind biased treatments near coarse-fine interfaces have also been successfully used for LES of both wall-bounded turbulence[118], and compressible and variable density turbulence[22]. The reader is referred to the work by Tu et al.[125] for a broader discussion of upwind biased discretizations for treatment of numerical instabilities arising on patched grids.

1.3 GRID STAGGERING AND FLUX EVALUATIONS

Prior to reviewing popular finite difference discretization choices, certain fundamental ideas regarding dependent variable placement (storage) patterns, as well as two distinct flux evaluation strategies that exist for more widely used collocated-grid formulations are introduced. The strategies discussed herein address a very important requirement for schemes used in turbulence simulations: non-linear stability and robustness.

1.3.1 Primitive variable placement

Two popular choices for dependent variable storage are shown in Figure 1.5. The first pattern, commonly referred to as *collocated grid pattern* requires that all dependent variables be stored/placed at grid locations referred to as *nodes*. The second pattern, requires certain thermodynamic variables (such as density and pressure) to be placed at grid nodes, while the kinematic variables such as (velocities or momenta) are stored/placed at half-points, also referred to as *midpoints*. Note that while other variable placement patterns involving partial staggering (such as pressure-velocity staggering for incompressible flow and Arakawa-variations for compressible flow) exist, we will primarily focus on the two strategies depicted for brevity since the principal arguments can be extended to other storage patterns in a straightforward manner. While the collocated placement/storage pattern tends to be substantially more programming-friendly than the staggered placement/storage pattern, there are several inherent non-linear stability advantages to the staggered grid pattern. Compressible-flow Navier-Stokes equations contain momentum fluxes with a triple product (cubic non-linearity) whereas the incompressible flow equations contain quadratic non-linearities introduced via the convective momentum flux as well as the source term of the Poisson equation for pressure. This implies that any energy content in primitive variables at wavenumbers beyond $k = 1/2k_{\mathrm{Nyq}}$ for compressible flow formulations, and beyond $k = 2/3k_{\mathrm{Nyq}}$ for incompressible flow formulations result in aliased fluxes. This is where a major advantage of the staggered grid formulation is apparent.

1. **Inviscid Flux: Lower aliasing errors in staggered formulations.** In the staggered storage pattern, the momentum fluxes are evaluated at the nodes while the momentum PDEs are evolved at mid points; the flux evaluation at the nodes requires interpolation of variables from midpoints to node centers. As shown in Figure 1.6, the interpolation kernels act as low-pass filtering operators in spectral space. Thus the fields that make up the non-linear flux get individually *de-aliased* prior to flux evaluation. The divergence of flux operator is a staggered first derivative operator which simply preserves the high-wavenumber content within the flux. This is not true for conventional discretizations on collocated grids where fluxes are also nodal (algebraic) and as such aliased. Since transport in LES and DNS is dominated by

convective processes (unlike in RANS using eddy viscosity closures where viscous transport dominates), robust formulation of the inviscid fluxes underpin non-linear robustness. Nagarajan et al.[143] demonstrated robustness of staggered formulations using high-order compact finite difference schemes and compared with collocated formulations which were shown to be unstable for high Reynolds number homogeneous isotropic turbulence simulations. This staggered formulation was later used for high-Reynolds number LES in a variety of academic and industrial applications[144,145] using curvilinear grids.

2. **Viscous Flux: Improved spectral resolution in staggered grid formulations.** In fluid simulations employing Newtonian viscous stress, the (viscous) flux requires first derivative evaluations. Since viscous stress in both DNS/LES and RANS using eddy-viscosity closures is primarily dissipative in character (acting to smooth out local gradients), it is of utmost interest to resolve the high-wavenumber content in these stresses. Again, the natural use of staggered derivative operators necessitated by the staggered storage pattern achieves this while the collocated storage pattern lacks any high-wavenumber content in the viscous fluxes due to the filtering effect of collocated derivative operators.

Throughout this section we will consider four-types of 5-stencil point wide operators and their spectral representations which are shown in Figure 1.6.

1. Collocated first derivative operator:

$$\alpha f'_{j-1} + f'_j + \alpha f'_{j+1} = a\frac{f_{j+1} - f_{j-1}}{2\Delta_x} + b\frac{f_{j+2} - f_{j-2}}{4\Delta_x} \tag{1.31}$$

where f'_j is the derivative at the jth node with a corresponding modified wavenumber, k' (see Chapter 1 for definition):

$$k'(k) = \frac{a\sin(k) + (b/2)\sin(2k)}{1 + 2\alpha\cos(k)} \tag{1.32}$$

2. Staggered first derivative operator:

$$\alpha f'_{j-1} + f'_j + \alpha f'_{j+1} = a\frac{f_{j+1/2} - f_{j-1/2}}{\Delta_x} + b\frac{f_{j+3/2} - f_{j-3/2}}{3\Delta_x} \tag{1.33}$$

and the corresponding modified wavenumber given as:

$$k'(k) = \frac{2a\sin(k) + (2b/3)\sin(3k/2)}{1 + 2\alpha\cos(k)} \tag{1.34}$$

3. Midpoint-node interpolation operator:

$$\alpha f^I_{j-1} + f^I_j + \alpha f^I_{j+1} = a\frac{f_{j+1/2} + f_{j-1/2}}{2} + b\frac{f_{j+3/2} + f_{j-3/2}}{2} \tag{1.35}$$

where f_j^I is the interpolation of the function f known at the midpoints to the jth node; with a corresponding transfer function:

$$T(k) = \frac{a\cos(k/2) + b\cos(3k/2)}{1 + 2\alpha\cos(k)} \tag{1.36}$$

4. Collocated second-derivative operator (not directly used in Navier-Stokes discretizations):

$$\alpha f''_{j-1} + f''_j + \alpha f''_{j+1} = a\frac{f_{j+1} - 2f_j + f_{j-1}}{2\Delta_x^2} + b\frac{f_{j+2} - 2f_j + f_{j-2}}{4\Delta_x^2} \tag{1.37}$$

where f''_j is the second derivative at the jth node. The modified wavenumber for the second derivative is computed as:

$$k''(k) = \frac{2a(1 - \cos(k)) + (b/2)(1 - \cos(2k)}{1 + 2\alpha\cos(k)} \tag{1.38}$$

Operators with $\alpha = 0$ are referred to as *explicit* finite difference operators, whereas those with $\alpha \neq 0$ are *Pade*-type finite difference operators. While the shortcomings of collocated storage pattern are well understood, the vast majority of scale resolving simulation utilizing finite difference discretizations (especially with higher order schemes) employ collocated variable storage patterns using collocated derivative operators due to implementation simplicity. However, when these algorithms are applied for LES (as opposed to DNS) in high Reynolds number settings, they invariably require additional stabilization such as explicit filtering, artificial selective-damping or hyperviscosity to achieve non-linear robustness even in flows lacking physical stiffness associated with shock waves or density interfaces (see for example filters proposed in [5,6]). In LES utilizing explicit SGS closures, this is undesirable - due to lack of quantifiable turbulent kinetic energy dissipation resulting from explicit filtering as well as due to ambiguity of filtering on generalized curvilinear grids. While both flaws of the collocated storage pattern when used with compressible Navier-Stokes formulations can be addressed via careful flux evaluation strategies (as discussed in the next subsection), this is unfortunately not true for the incompressible Navier-Stokes formulation as is discussed later in Section 1.6.

1.3.2 Staggered flux evaluations in collocated variable formulation

Robust variants of collocated variable storage schemes for treatments of the viscous and the inviscid fluxes are discussed separately since the objectives of each are distinct. Figure 1.7 depicts two fourth order accurate inviscid (Euler) flux discretizations that are purely central with no-upwind bias. We will refer to schemes that exclusively evaluate fluxes at solution nodes as Type A schemes whereas, schemes that utilize fluxes at midpoints followed by a divergence operator applied either exclusively to the midpoint fluxes (second order

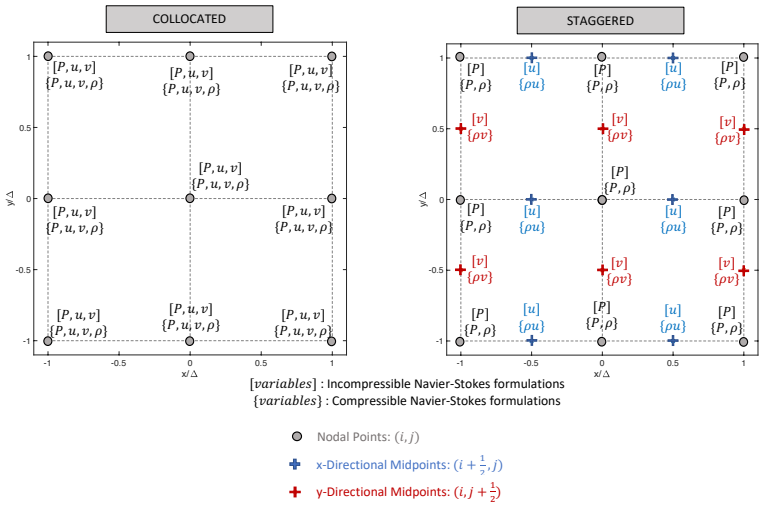

FIGURE 1.5 Two of the most common variable-storage patterns for Navier-Stokes (illustrated for the two-dimensional Cartesian grid case). Compressible Navier-Stokes solvers typically utilize two thermodynamic variables (out of ρ, P and T) depending on boundary conditions and equation of state preferences. For the staggered storage pattern, the mass and total energy equations are evolved on the *nodal* points, whereas the individual components of the vector momentum are evolved on their respective directional *midpoints* in compressible flow solvers.

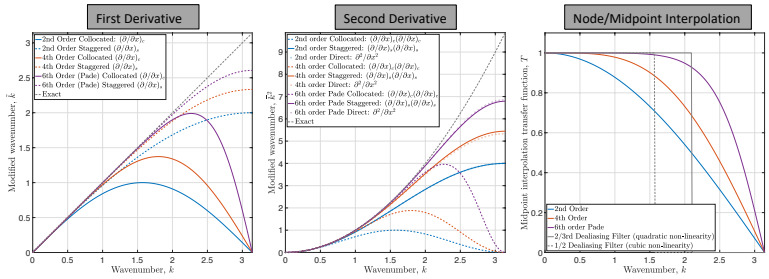

FIGURE 1.6 Spectral space representation of finite difference errors for various operators needed for discretization. While classical collocated storage formulation only employs collocated operators throughout the discretization, the staggered storage formulations require use of both staggered derivative operators as well as interpolation operators.

Scheme	α	a	b	Equation
Second Order				
├─Interpolation	0	1	0	Eq. 1.35
├─Collocated First Derivative	0	1	0	Eq. 1.31
├─Staggered First Derivative	0	1	0	Eq. 1.33
└─Second Derivative	0	1	0	Eq. 1.37
Fourth Order				
├─Interpolation	0	9/8	−1/8	Eq. 1.35
├─Collocated First Derivative	0	4/3	−1/3	Eq. 1.31
├─Staggered First Derivative	0	9/8	−1/8	Eq. 1.33
└─Second Derivative	0	4/3	−1/3	Eq. 1.37
Sixth Order Pade				
├─Interpolation	3/10	3/2	1/10	Eq. 1.35
├─Collocated First Derivative	1/3	14/9	1/9	Eq. 1.31
├─Staggered First Derivative	9/62	63/62	17/62	Eq. 1.33
└─Second Derivative	2/11	12/11	3/11	Eq. 1.37

TABLE 1.1 Coefficients for Finite Difference schemes depicted in Figure 1.6

accurate in the illustration) or a combination of both midpoint and nodal fluxes (fourth order accurate in the illustration) as Type B. These midpoint-and-node (MND) operators[20,180] (discussed in more depth in Section 1.4.2.1) should be interpreted as regular staggered finite difference operators applied for a field at $\Delta/2$ spacing and as such have excellent spectral properties similar to regular staggered finite difference operators. The kinetic energy and entropy preserving discretizations that are discussed in Section 1.4.1 can be characterized as Type B schemes since the underlying principle is to construct flux approximations at midpoints with subsequent use of staggered derivative operators for the divergence of midpoint fluxes. When the midpoint fluxes shown for Type B Scheme in Figure 1.7 are computed via 4th order interpolation of primitive variables at the midpoints, followed by a 4th order accurate midpoint-and-node (MND) derivative operator for divergence of the fluxes, an overall 4th order accurate discretization is obtained similar in truncation error convergence order to the conventional Type A scheme. This 4th order accurate midpoint-and-node flux derivative at the jth node is given as:

$$\left(\frac{\partial F}{\partial x}\right)_j = \frac{4}{3}\frac{F_{j+1/2} - F_{j-1/2}}{\Delta_x} - \frac{1}{6}\frac{F_{j+1} - F_{j-1}}{\Delta_x} \tag{1.39}$$

While for linearized Euler equations (small perturbations to a base state), the two schemes are mathematically identical and as such share identical linear stability

properties, the Type B scheme has far superior non-linear stability properties. While this linear scheme does not discretely preserve kinetic energy (in the low Mach limit) or the entropy, it still has very favorable stability characteristics suitable for high Reynolds number LES, provided that appropriate care is taken to discretize the subgrid scale viscous fluxes to ensure that viscous/SGS terms contribute finite damping at the Nyquist wavenumber. It is further relevant to point out that while the 4th order Type B scheme does require more floating-point operations (due to interpolated variables and additional midpoint flux evaluations), the total memory need for both schemes is identical and as such when implemented appropriately (using techniques such as cache-blocking), the computational costs of the 4th order Type B scheme is only marginally higher than that of the 4th order Type A scheme. Finally, note that for linear problems Type B schemes offers no obvious advantage over Type A schemes - in fact for linear problems the implied advection operator of the Type B scheme is simply the convolution of the interpolation operator and the staggered divergence operator. In wave-space this implies that the effective modified wavenumber for the Type B scheme is the product of the transfer function associated with the interpolation transfer function and the modified wavenumber associated with the staggered divergence operator. An important consequence of this interpretation for linear problems is that many of the optimized Type A explicit finite difference schemes (such as the DRP scheme) can be cast as Type B schemes via an appropriate choice of interpolation and staggered divergence operators using simple truncation error analysis and application the constraints for the order of accuracy to solve for coefficients of each operator. While the illustration shown in Figure 1.7 only considers the one-dimensional discretization over a uniformly spaced grid, the scheme can be trivially extended to the three-dimensional generalized curvilinear formulation introduced in Section 1.2.1. The main caveat is that for curvilinear grids, even linearized Navier-Stokes solutions can experience robustness issues due to poor grid quality which results in inaccurate metric terms. Here again, Type B discretizations can mitigate stability problems seen in Type A schemes which usually require use of spatial filtering to obtain stability[6]. This aspect is illustrated in a subsequent section of this chapter by considering advection of on an isentropic vortex on a wavy grid.

In order to formulate a viscous flux operator preserving high spectral resolution, consider the following simplification to the divergence of the viscous flux. Here we assume spatially constant shear and bulk viscosities, μ and μ_b respectively, although spatially variable viscosities (due to thermal variations at higher Mach numbers or due to utilization of Boussinesq type subgrid scale closures) can be treated with additional terms.

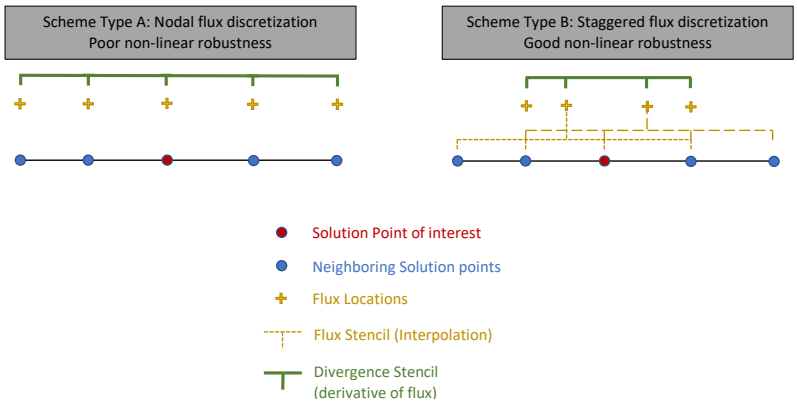

FIGURE 1.7 Two types of 4th order accurate inviscid flux discretizations using identical stencil widths. Note the staggered schemes use symmetric stencils. The midpoint-and-node derivative operator in Scheme B is given in Equations 1.39.

$$\nabla \cdot \left(2\mu \boldsymbol{S} + \left(\mu_b - \frac{2}{3}\mu\right)(\nabla \cdot \boldsymbol{u})\boldsymbol{I}\right) = \mu \nabla \cdot (2\boldsymbol{S}) + \left(\mu_b - \frac{2}{3}\mu\right)\nabla(\nabla \cdot \boldsymbol{u}) + \text{additional terms involving } \nabla\mu \text{ and } \nabla\mu_b \quad (1.40)$$

where $\boldsymbol{S}$ is the strain rate tensor defined as $\frac{1}{2}\left(\partial_i u_j + \partial_j u_i\right)$. With further rearrangement we obtain

$$\mu \nabla \cdot (2\boldsymbol{S}) + \left(\mu_b - \frac{2}{3}\mu\right)\nabla(\nabla \cdot \boldsymbol{u}) = \mu \nabla^2 \boldsymbol{u} + \lambda \nabla(\nabla \cdot \boldsymbol{u}) \quad (1.41)$$

where $\lambda = \left(\mu_b + \frac{1}{3}\mu\right)$. Now, let us consider two second order discretizations shown in Figure 1.8. It is straightforward to show that the two discrete analogs (assuming constant μ and μ_b) for the right-hand side of Equation 1.41 for the two schemes are:

Scheme A:

$$\text{RHS}_{i=1} = \mu \partial_j^{(c)} \left[\partial_j^{(c)} u_1\right] + \lambda \partial_1^{(c)} \left[\left(\partial_m^{(c)} u_m\right)\right] \quad (1.42)$$

Scheme B:

$$\text{RHS}_{i=1} = \mu \partial_j^{(s)} \partial_j^{(s)} u_1 + \lambda \partial_1^{(s)} \left(\partial_1^{(s)} u_1 + \mathcal{I}^{n \to m}\left\{\partial_2^{(c)} u_2 + \partial_3^{(c)} u_3\right\}\right) \quad (1.43)$$

where, the discrete collocated and staggered derivative operators are given by $\partial^{(c)}$ and $\partial^{(s)}$ respectively, and $\mathcal{I}^{n \to m}$ is the interpolation operator from nodes to

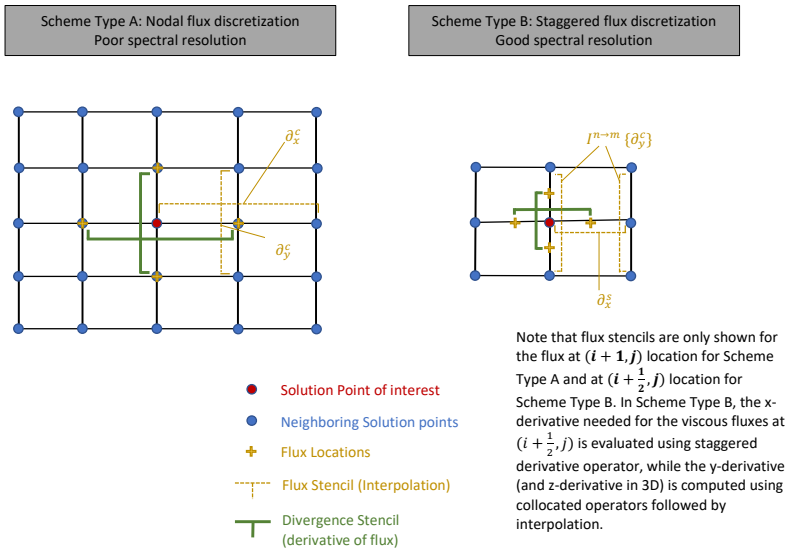

FIGURE 1.8 Two types of 2nd order accurate flux discretizations. Type B Scheme ensures that the net viscous (force) due to vortical velocity is nonzero at Nyquist wavenumber. This is not true for Scheme A even though it uses a larger/wider stencil.

midpoints. At this time, it is apparent that while Scheme A uses a wider stencil than Scheme B, the Scheme A operator's spectrum (or effective wavenumber) goes to zero at the Nyquist wavenumber. On the other hand, Scheme B preserves the high spectral resolution from the first term (by utilizing purely staggered operators) even though the dilatation calculation partially utilizes collocated operators and hence also has a spectrum that goes to zero at the Nyquist wavenumber. This substantially superior spectral character makes utilization of Scheme B a necessity in high-Reynolds number turbulence LES. Scheme A does not provide the necessary robustness and many such implementations resort to either additional filtering and/or hyperviscosity[82,83] or evaluation of viscous transport in non-conservative forms[80,81] to obtain robustness through the viscous terms.

Note in addition that for using the more robust Scheme B in LES, the subgrid scale model needs to be evaluated at mid-points as opposed to nodes to preserve the robustness advantages, which adds to its cost.

1.4 ROBUSTNESS OF INVISCID FLUX DISCRETIZATION

1.4.1 Linear Schemes

1.4.1.1 kinetic Energy preservation and Entropy consistency

Beyond the mass, momentum and total energy conservation implicit in the Euler equations, the kinetic energy (in the inviscid limit) is constrained by

$$\partial_t \left(\rho u_m u_m/2\right) + \partial_i \left(\left(\rho u_m u_m/2 + p\right) u_i\right) + p\partial_i u_i = 0 \tag{1.44}$$

where the pressure dilatation term, $p\partial_i u_i$ represents the reversible exchange between internal energy and kinetic energy (the sum of the two is a conserved quantify). Since the pressure-dilatation term vanishes in the low-Mach limit, the conservation of total kinetic energy follows. Thus, if the domain boundaries are periodic or contain walls (with only the inviscid requirement $\boldsymbol{u} \cdot \boldsymbol{n} = 0$) the domain integrated kinetic energy has to stay bounded. Given the positivity requirement for kinetic energy (assuming $\rho > 0$), many efforts beginning with Feiereisen[48][3] have proposed finite difference formulations that obey this kinetic energy conservation property in a discrete sense in order to obtain schemes that are provably non-linearly stable. A second source of inspiration for attaining non-linear robustness is Harten's[51] result:

$$\partial_t \left(\rho f(s)\right) + \partial_i \left(\rho f(s) u_i\right) = 0 \tag{1.45}$$

showing that any arbitrary differentiable function, $f(s)$ of the thermodynamic entropy, $s = \log(p/\rho^{-\gamma})$ is conserved. Validity of the conservation law in Equation 1.45 is only violated at shock-waves and contact discontinuitites and the reader is referred to texts by Lax[50] and LeVeque[49] for entropy-consistency requirements in such flows. However, finite difference schemes that satisfy the entropy constraint in flows without shocks or contact discontinuities are desirable to enhance robustness. Most efforts towards this end have focused on split-form discretization of the convective terms in Euler equations[52]. Two prominent examples of the proposed forms for momentum equations include:

Blaisdell et al. (1996)[53], Honein & Moin (2008)[56] and Jameson (2008)[55]:

$$\partial_t \left(\rho u_i\right) + 1/2 \left(\partial_j \left(\rho u_i u_j\right) + u_i \partial_j \left(\rho u_j\right) + \rho u_j \partial_j u_i\right) + \partial_i p = 0 \tag{1.46}$$

and

Kennedy & Gruber (2008)[54] and Kuya et al. (2018)[57]:

$$\begin{aligned}\partial_t \left(\rho u_i\right) + 1/4 \big(&\partial_j \left(\rho u_i u_j\right) + u_i \partial_j \left(\rho u_j\right) + u_j \partial_j \left(\rho u_i\right) \\ &+\rho u_i \partial_j u_j + \rho u_j \partial_j u_i \; + u_i u_j \partial_j \rho + \rho \partial_j \left(u_i u_j\right)\big) + \partial_i p = 0\end{aligned} \tag{1.47}$$

3. Arakawa (1966)[141] originally solved the incompressible Navier-Stokes equations using a vorticity-streamfunction formulation that preserved kinetic energy and enstrophy enabling stable long-time numerical integration for the first time.

While both quadratic (Eq. 1.46) and cubic (Eq. 1.47) forms were utilized by various authors, the primary difference between them is the discretization of the energy equation. Blaisdell et al.[53] and Honein & Moin[56] solved the internal energy equation instead of the total energy equation, with the latter utilizing entropy directly in the formulation. The quadratic split form implies a kinetic energy preservation (KEP) at a semi-discrete level for periodic boundary conditions, while a summation-by-parts property is needed with non-periodic boundary conditions[59]. Kennedy & Gruber[54] performed aliasing analysis to demonstrate that the cubic form offers additional robustness when density fluctuations are stronger. While the quadratic-split form has often incorrectly been referred to as *skew-symmetric* form, Morinishi[60] performed the analysis to derive the convective splitting operators that satisfy the mathematical property of skew-symmetry.

In a recent work, Kuya, Totani & Kawai[57] argue that entropy consistency required the finite difference formulation to satisfy the following three properties: a) Discrete kinetic energy equation needs to be derived from the discrete mass and momentum equations, b) Discrete convective velocity for internal energy and kinetic energy need to be identical, and c) the discrete analog of the product rule from pressure diffusion: $\partial_j(pu_j) = p\partial_j u_j + u_j\partial_j p$ must hold. Subsequently, they proposed a consistent discretization of the total energy equation which showed excellent entropy conservation properties (KEEP). Shima et al.[61] later showed that all KEP and KEEP schemes suffered from unphysical pressure oscillations for purely entropic modes (u and p constant, ρ spatially varying) and proposed a modification to internal energy discretization that addressed this issue and thus provided additional robustness.

Two challenges remain prior to implementation of the split forms shown in Equation 1.46 and 1.47. These involve the lack of discrete conservation of mass, momentum and energy (the analytic product rule assumed is not discretely satisfied in general) and the increased computational cost; since the (split) forms require substantially more derivative operations than a conventional discretization in conservative form. The conservation property is particularly important in the context of the Lax-Wendroff theorem[62] which requires schemes to satisfy the telescoping property of the discrete divergence operator to guarantee convergence of the numerical solutions to the weak solutions of Euler Equations. Both these challenges were addressed by Ducros et al.[64] and Pirozzoli[63].

Consider a second order central difference discretization of the cubic split form:

$$\frac{\partial \rho\phi u}{\partial x} = \frac{1}{4}\Bigg[\frac{(\rho\phi u)_{i+1} - (\rho\phi u)_{i-1}}{2\Delta x} + u_i \frac{(\rho\phi)_{i+1} - (\rho\phi)_{i-1}}{2\Delta} + (\rho\phi)_i \frac{u_{i+1} - u_{i-1}}{2\Delta} + \phi_i \frac{(\rho u)_{i+1} - (\rho u)_{i-1}}{2\Delta} + (\rho u)_i \frac{\phi_{i+1} - \phi_{i-1}}{2\Delta} + \rho_i \frac{(u\phi)_{i+1} - (u\phi)_{i-1}}{2\Delta} + (\phi u)_i \frac{\rho_{i+1} - \rho_{i-1}}{2\Delta}\Bigg] \quad (1.48)$$

Ducros et al.[64] showed that expressions of this form can be written in flux form as:

$$\frac{\partial \rho\phi u}{\partial x} = \frac{\tilde{F}|_{i+\frac{1}{2}} - \tilde{F}|_{i-\frac{1}{2}}}{\Delta x} \quad (1.49)$$

where the approximate fluxes at the midpoints are given by:

$$\tilde{F}_{i\pm\frac{1}{2}} = \frac{\rho_i + \rho_{i\pm1}}{2}\frac{\phi_i + \phi_{i\pm1}}{2}\frac{u_i + u_{i\pm1}}{2} \quad (1.50)$$

Subsequently, Pirozzoli[63] showed that an arbitrarily higher order split-form KEP scheme can be constructed using the flux form given in Equation 1.49 as:

$$\tilde{F}_{i\pm\frac{1}{2}} = 2\sum_{l=1}^{L} a_l \sum_{m=1}^{l-1} \left(\widetilde{\rho, \phi, u}\right)_{i\mp m, \pm l} \quad (1.51)$$

where the coefficients are the general explicit finite difference coefficients (of arbitrary order or spectral resolution determined by the stencil size 2L+1) and the cubic product operator is given as:

$$\left(\widetilde{\rho, \phi, u}\right)_{j,l} = \frac{\rho_j + \rho_{j+l}}{2}\frac{\phi_j + \phi_{j+l}}{2}\frac{u_j + u_{j+l}}{2} \quad (1.52)$$

It is now clear why high order KEP and KEEP schemes fall within the subset of *reduced aliasing forms* referred to as Type B schemes shown in Figure 1.7. While Pirozzoli's result[63] (Eq. 1.52) when combined with energy equation split form of Kuya et al.[57] allows construction of explicit finite difference KEEP schemes of arbitrarily high order, the flux form expressions cannot be determined for implicit Pade-type schemes. However, recent work by Song et al.[11] has shown that substantial robustness (due to reduced aliasing errors) can be achieved via utilization of staggered Pade derivative and interpolation operators in a Type-B inviscid flux discretization. The KEEP schemes have also been proposed for generalized curvilinear grids[47] using higher order accurate explicit finite difference discretizations. The authors also provide evidence of KEEP property using standard sixth order compact finite difference scheme[2]

when each term of the split form is separately evaluated using the compact derivative operator. Unfortunately, such a scheme cannot be cast into Ducros et al.[64] conservation form. Before concluding the discussion of KEP and KEEP discretizations, two important attributes of such schemes need to be noted. Firstly, while such schemes preserve kinetic energy in the inviscid low Mach number limit, the resulting solutions will suffer from significant energy pile-up near Nyquist scales if no subgrid scale closure is used since the kinetic energy transfer associated with the inviscid fluxes is non-dissipative. Furthermore, at the time of this writing, majority of the past applications using high-order accurate KEEP schemes to wall-turbulence LES seem to require additional de-aliasing filtering for robustness[47,65]. Second, the schemes discussed above only conserve kinetic energy in a semi-discrete sense (at low-Mach numbers); as such temporal discretization errors are pertinent and most numerical investigations only study the properties at low CFL numbers (< 0.1) that are not representative of real applications[57]. Recent work by Jain & Moin[146] has extended KEEP schemes for compressible two-phase flows.

1.4.2 Flows with discontinuities

Euler equations exhibit a tendency to form steep gradients - shock waves and contact discontinuities. For a shock wave associated with a supersonic mean flow Mach number, M with incident turbulence described in terms of its turbulent Mach number, $M_t = \left\langle u_i' u_i' \right\rangle / \langle c \rangle$ (where $\langle c \rangle$ is the speed of sound and u_i' is the fluctuation velocity), and its Taylor Microscale Reynolds number, Re_λ, the ratio of the shock thickness and the Kolmogorov scale has the following proportionality[159]

$$\frac{\eta}{\delta_{\text{shock}}} \propto \frac{\mathrm{Re}_\lambda^{1/2}(M-1)}{M_t} \tag{1.53}$$

As such, for the vast majority of high Reynolds number cases, $\eta \gg \delta_{\text{shock}}$ and resolution of steep gradients associated with the shocks is computationally intractable in most LES and DNS[4] settings. Historically, numerical treatment of such discontinuities has focused on schemes with favorable monotonicity preservation and total deviation diminishing (TVD) properties[66,68,70]; a major advantage of such discretizations is the availability of mathematical proofs showing convergence to unique entropy-consistent weak solution[69]. However, as shown by Harten et al.[70] such TVD schemes are at most first order accurate and suffer from loss of accuracy in both smooth and non-smooth regions of the flow which makes them unsuitable for use in scale-resolving simulations. Over the past two decades, a vast array of literature specifically targeting numerical discretizations for shock and interface capturing in scale-resolving flows has emerged and a comprehensive review is beyond the scope of this chapter. The

4. The definition of the DNS is somewhat ambiguous in such situations; here we refer to DNS as simulations that resolve all vortical fluctuations up to the Kolmogorov scale.

reader is referred to the work by Garnier et al.[71] and Larsson et al.[72] for assessment of shock-capturing schemes in LES, and the work by Pirozzoli[73] for a discussion of spectral characteristics of shock-capturing schemes. In the following, we provide a brief overview of two distinct approaches for scale-resolving simulations of turbulent flows in the presence of shocks.

1.4.2.1 Non-linear Schemes: WENO interpolation and WCNS

Over the past few decades, finite difference WENO schemes and Weighted Compact Non-linear schemes (WCNS) have emerged as the two most popular choices for LES of flows with strong discontinuities. We will primarily focus on the WCNS formulation in this chapter because of certain advantages its proponents claim it has over finite difference WENO schemes[20]: a) WCNS is generally considered to have better spectral properties[96], b) it allows for large flexibility in regards to the specific flux formulation at the midpoints (common fluxes including Roe's flux difference splitting form[93], Toro's HLLC flux[94] or Liou's AUSM flux[95] are all possible depending on their respective trade-offs), and c) the method can be very conveniently extended to generalized curvilinear formulations of arbitrarily high order[10,96]. As introduced by Deng & Zhang[3], these schemes in general comprise of three steps:

1. Non-linear interpolation from nodes to mid-points. In this first step, characteristic transform is performed on conserved variables to obtain characteristic variables. The left and right biased interpolations are used to obtain characteristic variables at midpoints. WENO candidate stencils are utilized for this interpolation. Since the original upwind-biased non-linear weights proposed by Jiang and Shu[4], several variations have been proposed specifically aimed at reducing numerical dissipation in *smoother* regions of the flow in order to better distinguish shocks from high-wavenumber vortical and acoustic fluctuations present in large Reynolds number LES. These improvements primarily rely on additional sub-stencils and the selection of non-linear weights to improve spectral characteristics of the interpolation to increase resolution in smooth flows [97–100,157]. Note that over the past decade, resolution characteristics of WCNS's have been greatly improved almost exclusively via improvements to the non-linear interpolation.
2. Midpoint flux evaluation. In this second step, the left and right biased characteristic variables are transformed to conservative variables for flux evaluation. Since the exact solution to the generalized Riemann problem is computationally expensive, approximate Riemann solvers originally proposed for Godunov-type schemes are utilized. Note that the consistency condition for approximate Riemann solvers implies that given identical left- and right-biased interpolations, the effective mid-point flux is purely non-dissipative. This is also the step where positivity-preservation can be enforced by appropriate blending with the Lax-Friedrichs flux[103] or other positivity-preserving fluxes[100] for simulation of flows in extreme condi-

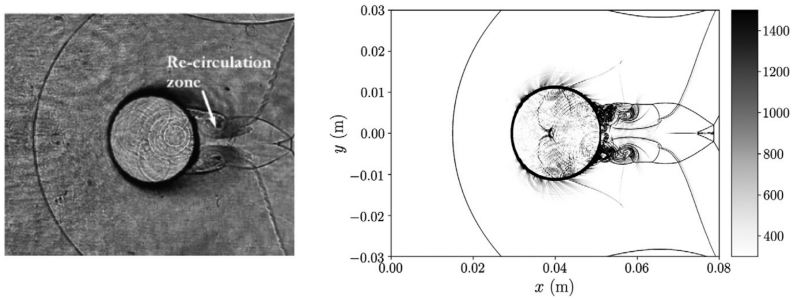

FIGURE 1.9 Density gradient magnitude (right) from a 2D simulation of a Mach 2.4 shock-wave interacting with a water column performed using a positivity-preserving scheme[75] compared against experimental shadowgraph (left) by Sembian et al.[139]. Figure reproduced from Wong et al.[75] with authors' permission.

tions.

3. Flux derivative evaluation. A central finite difference derivative is typically used to evaluate the flux derivative. Nonamura & Fujii[20] showed that mid-point and node schemes that combine the approximate (upwind-biased) midpoint fluxes with nodal (exact) fluxes offer superior robustness compared to simple staggered midpoint derivatives. Since this work, many higher order extensions including utilization of Pade-type operators have been proposed for computing the derivative of the flux[3,151].

In a recent work, Tian et al.[179] addressed the effectiveness of shock-capturing simulations in studying the canonical shock-turbulence interaction (STI) problem. They utilized

Non-linear schemes such as WCNS have been very successful for simulation of extreme flows (high density ratios and Mach numbers) in part due to recent extensions for obtaining positivity preserving characteristics[75,84,100–104]. Figure 1.9 shows one such application of WCNS for simulation of high-Mach number multiphase flows.

1.4.2.2 Artificial dissipation

Regularization of discontinuities via damping terms dates back to the work of von Neumann & Richtmyer[106] who proposed the utilization of source diffusion terms with coefficients $c \propto h^2 \left|\partial_x u\right|$. Since then two classes of methods utilizing artificial dissipation have emerged.

The first such method was introduced by Jameson et al.[107] where the midpoint fluxes are augmented as:

$$\boldsymbol{F}_{i+1/2} = \boldsymbol{F}^{\text{central}}_{i+1/2} + \boldsymbol{F}^{\text{AD}}_{i+1/2} \tag{1.54}$$

where $\boldsymbol{F}^{\text{central}}_{i+1/2}$ is a non-dissipative flux (that could come from a KEEP scheme

for example) and the additional term $\boldsymbol{F}^{\mathrm{AD}}_{i+1/2}$, which takes the form:

$$\boldsymbol{F}^{\mathrm{AD}}_{i+1/2} = a_{i+1/2}\left(-\varepsilon^{(2)}_{j+1/2}\left(\boldsymbol{W}_{i+1}-\boldsymbol{W}_i\right) + \varepsilon^{(4)}_{j+1/2}\left(\boldsymbol{W}_{i+2}-3\boldsymbol{W}_{j+1}+3\boldsymbol{W}_j-\boldsymbol{W}_{j-1}\right)\right) \quad (1.55)$$

where $a_{i+1/2}$ is the spectral radius of the inviscid flux Jacobian matrix with Roe averaging[93], and $\boldsymbol{W}$ is the vector of conserved variables. The two coefficients, $\varepsilon^{(2)}$ and $\varepsilon^{(4)}$ are computed as

$$\varepsilon^{(2)}_{i+1/2} = \alpha_2\psi_{i+1/2} \ , \ \varepsilon^{(4)}_{i+1/2} = \max(0, \alpha^4 - \varepsilon^{(2)}_{i+1/2}) \quad (1.56)$$

where $\psi_{i+1/2}$ is a pressure sensor bounded between 0 and 1 and computed as:

$$\psi_{i+1/2} = \max(\psi_i, \psi_{i+1}) \ , \ \psi_i = \frac{|p_{i+1}-2p_i+p_{i-1}|}{|p_{i+1}+2p_i+p_{i-1}|} \quad (1.57)$$

The recommended values for global constants are $\alpha_2 = 1$ and $\alpha \approx 0.01 - 0.05$. Since the original scheme proposed by Jameson et al.[107] was intended for RANS, the second order term was designed to be non-zero only near shocks, while the fourth order term was intended to act as dealiasing. Pulliam[108] studied this formulation in the context of hybrid RANS/LES and used an additional sixth order term. Brehm et al.[109] investigated the dissipation characteristics of this type of artificial diffusivity in the context of LES and showed that the additional terms can be interpreted as 2nd, 4th and 6th order hyperviscosities. An analogous use of hyperviscosity for dealiasing for incompressible flow can be found in Lamballais et al.[105] who modified the viscous second derivative operator to obtain similar high-order damping properties utilizing Pade-schemes. The analogy between the second order dissipation terms and the Lax-Friedrichs flux is discussed in LeVeque[49].

The second class of methods for regularization via artificial diffusion is inspired by work of Tadmor[112] and Guo et al.[113] on spectrally accurate vanishing viscosity. Barone & Lele[140] presented the idea of using additional terms scaling with the sixth derivative $\propto \Delta_x^5 \frac{\partial^6 u}{\partial x^6}$ as a regularization - the motivation for 6th derivative stems from the fact that the additional term introduces a numerical error no worse than the dispersive error of the discretization scheme. Cook & Cabot[82] later generalized this by introducing high-wavenumber biased artificial fluid properties. This was later improved by Mani et al.[110] and Bhagatwala & Lele[111] for additional selectivity in regards to resolved acoustic motions. Kawai & Lele[76] further generalized the formulation for curvilinear coordinates. The artificial viscosities and thermal diffusivity are computed as:

$$\mu^\star = c_\mu\overline{\rho\left|\nabla^r F_\mu\right|}\Delta_x^{r+2} \ , \ \mu_v^\star = c_{\mu_v}\overline{\rho\left|\nabla^r F_{\mu_v}\right|}\Delta_x^{r+2} \ , \ \kappa^\star = c_\kappa\overline{\frac{\rho c_s}{T}\left|\nabla^r F_\kappa\right|}\Delta_x^{r+2} \quad (1.58)$$

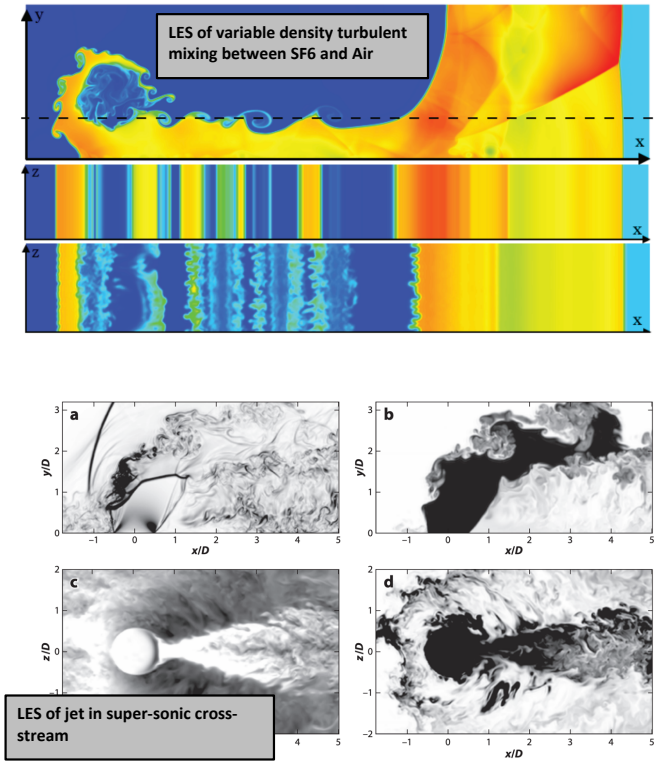

FIGURE 1.10 Examples of LES of high-Mach number turbulent flows performed using Localized Artificial Diffusivities (LAD) for shock capturing. The image of inclined interface multi-material Richtmeyer Meshkov mixing is taken from Subramaniam & Lele[77], while the image depicting jet in supersonic cross-flow is taken from Kawai & Lele[76].

where $\overline{(\cdot)}$ is a Gaussian filtering operator and F_μ, F_{μ_v} and F_κ are appropriately chosen kernels that are local functions of flow variables. The essence of such *Localized Artificial Diffusivity* (LAD) approaches is ability of the high order Laplacian operator ($\nabla^r, r > 4$) to detect sharp gradients associated with shocks and contact interfaces, and to locally enhance the viscosity/diffusivity. As such, most applications of this method have relied on use of high-order schemes with good spectral properties (such as Pade schemes) to compute the Laplacian operators. This approach has been demonstrated to be very versatile with extensions to multicomponent mixtures[115] as well as in the study of elastic-plastic deformations in solids[114]. Two examples utilizing LAD based shock capturing are shown in Figure 1.10.

1.5 FINITE DIFFERENCE SCHEMES FOR LES: DISPERSION/DISSIPATION ERRORS

1.5.1 Are low-dispersion error schemes relevant for LES in turbulence-dominated flows?

Significant work has been done in the past three decades in optimization of finite difference stencils to attain very favorable spatio-temporal dispersion error characteristics[1,2,5,31]. Some of this is motivated by aeroacoustics[32,33] where direct numerical propagation of sound waves to large distances requires time integration of a linear hyperbolic process. In such applications, minimization of both dispersion as well as dissipation errors is necessary since both the amplitude as well as phase of the propagating waves are of importance. Similarly, in flows dominated with linear phenomena (such as boundary layer and shear-layer instabilities), improving spectral characteristics of the numerical discretization leads to obvious improvements in solution accuracy. Historically, direct numerical simulations of a variety of turbulent flows (including those involving wall-turbulence) have been performed using high-order accurate (low-truncation error) discretizations (see example in [34–37]). However, the benefit of low-dispersion error discretizations in Large Eddy Simulations at high Reynolds numbers is far from established[43] and appropriately discretized second order (such as Type B) schemes have enjoyed tremendous success in both academic as well as engineering problems. Vast majority of high-Reynolds number geophysical and engineering wall-bounded flows (including those involving stratification) are simulated using second or fourth order discretizations[40–42] with majority of numerical improvements focused on improving subgrid-scale closures and wall-boundary condition treatments. Success of second order schemes in LES is not only limited to wall-bounded turbulence; second and fourth order staggered LES discretizations on curvilinear grids have also been reported in jet aeroacoustics[44,85], although part of this success has to do with utilization of acoustic analogies such as Ffowcs Williams & Hawkings methods[181–183] for farfield noise predictions instead of direct numerical propagation.

Some insight into the success of second and fourth order discretizations for LES can be seen by considering the LES of homogeneous isotropic turbulence with linear forcing[46] at infinite Reynolds numbers. Figure 1.11 shows the energy spectrum at the equilibrium/stationary state for three Type-B discretizations - all utilizing Vreman's[45] subgrid scale closure. The spectral content in the simulation for the 6th order Pade discretization is only marginally improved compared to the standard 2nd order scheme. Recent work[47] comparing flat plate boundary layer LES makes a similar observation; essentially identical first and second order moments are predicted by LES performed using various KEEP schemes ranging from second up to eighth order of accuracy. All schemes produce statistics with equivalent accuracy as those obtained via LES using a sixth order Pade scheme with substantially superior dispersion error characteristics.

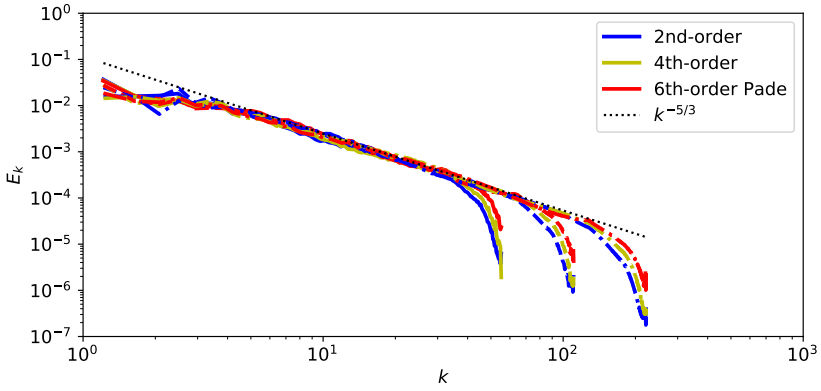

FIGURE 1.11 Kinetic Energy Spectrum for decaying homogeneous isotropic turbulence initialized with the von Karman spectrum, at $t\,\varepsilon_0/k_0 \approx 20$. Three different (Type-B) finite difference schemes are considered and Vreman's SGS model is utilized. Note that while the second order scheme is KEP and hence stable without an SGS model, both the fourth order and the sixth order Pade schemes are only stable with an SGS closure. The turbulent Mach number is approximately 0.07 and the simulation is performed in the limit $\mathrm{Re}_\lambda \to \infty$ using grid levels of 64^3, 128^3 and 256^3 in a $[2\pi]^3$ domain. Note that all Type-A schemes of equivalent order of accuracy are unstable without the use of explicit filtering. Figure generated by Hang Song (Stanford University).

This result (reproduced from [47]) is presented in Figure 1.12.

An interesting counter-argument regarding adequacy of second order discretizations for LES was made in a recent work by Yalla et al.[147]. The authors argue that mean-convection is ubiquitous in LES applications and as such the numerical dispersion error associated with mean convection of vortical motion (turbulence) can manifest as phase de-coherence in triadic interactions thereby affecting the inter-scale energy transfer rate. As such when linear dynamics associated with mean convection are dominant, higher-order discretizations that minimize disperion errors are still likely to be advantageous.

Now, let us consider a simpler linear advection problem with a band limited square-wave initial condition. Figure 1.13 considers both the discrete square wave defined via Heaviside functions as well as its band limited variant (spectrally filtered to retain wavenumbers up to $1/2$ Nyquist wavenumber) based on a 64-point discretization. This (spectrally sharp) regularization of the square wave produces Gibbs oscillations in the initial condition and in the exact solution. The 5 linear schemes considered are purely dispersive and as such cannot perform in a shock/discontinuity capturing mode for a discontinuous initial condition. The oscillations near a discontinuity are undesirable in capturing a weak-form solution, but the oscillations in the present band-limited problem (as shown in the top left panel of figure 1.13) are part of the solution. In the context of preserving the *phase* of transient waves, Figure 1.13 shows that superior spectral properties of higher order optimized schemes can lead to superior preservation

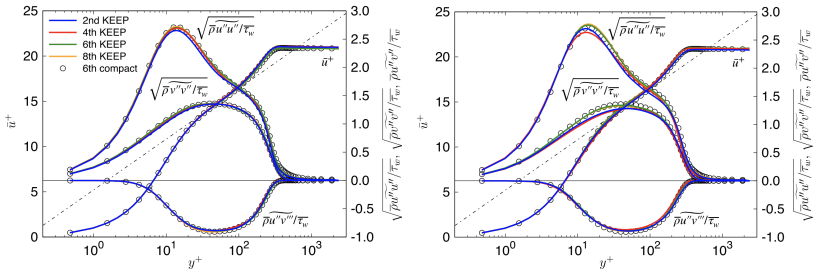

(a) Grid α (b) Grid β

FIGURE 1.12 First and second order single point correlations for LES of turbulent flat plate at $\mathrm{Re}_\theta = 750$, $\mathrm{Re}_\tau = 290$ and $M_\infty = 0.3$ for two different grid levels. Figure reproduced from Kuya & Kawai[47] with authors' permission.

of interfaces. Another advantage of schemes with superior spectral properties can be seen in simulations of curvilinear grids exhibiting large mesh skewness as shown in Figure 1.14. 6th order Pade discretization provides a substantially superior preservation of the initial vortex structure after 10 periods of advection compared to the 4th order scheme, which in turn is superior to the 2nd order accurate scheme.

Sharp interfaces occur commonly in both compressible and incompressible turbulent flows. Examples include density interfaces seen in Rayleigh-Taylor instability driven mixing problems (incompressible and compressible)[83], as well as turbulent mixing problems in stratified flows[40]. Other examples involving compressible turbulence include homogeneous compressible turbulence[86], compressible shear layers[87], supersonic channel flows and boundary layers[91], as well as problems involving shock-turbulence interaction[89] shock-boundary layer interactions[90] and Richtmyer-Meshkov instability[39,88]. The majority of these multi-physics DNS and LES applications involving variable density turbulence, interfacial mixing, and shock-turbulence interactions have utilized high-order discretizations. In such applications oscillations occurring near interfaces and discontinuities can cause non-linear instabilities due to the positivity requirement for various thermodynamic variables, and the benefits of shock-capturing discretizations start becoming relevant even in LES. A key consideration is balancing the need for wide band accuracy of wave propagation with the need for localized dissipation near discontinuities.

1.5.2 Are shock-capturing schemes suitable to be used for LES?

While the previous sections of this chapter have discussed importance of non-linear robustness and specific requirements for shock-capturing, it is natural to ask if the non-linear schemes (such as WCNS) that provide excellent shock-capturing traits along with promising spectral resolution (since the interpolation

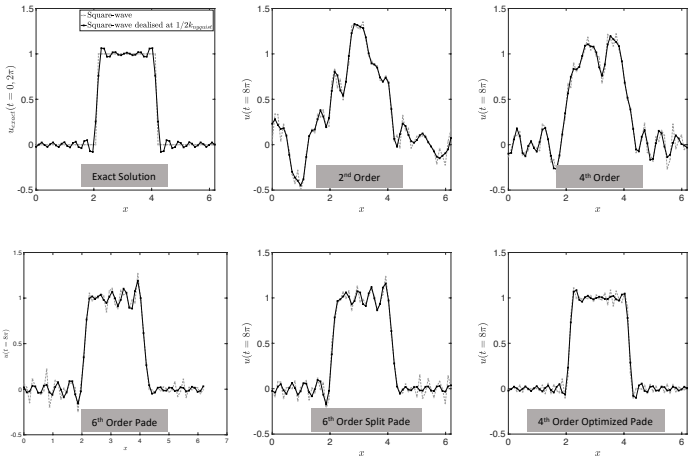

FIGURE 1.13 Solution to linear advection ($\partial_t u + \partial_x u = 0$) for square-wave type initial conditions , and periodic boundary conditions at $t = 8\pi$. The *Split Pade* scheme represents the Type-B (see Figure 1.7) 6th order Pade scheme[11] which provides superior non-linear robustness compared to both the standard collocated 6th order Pade Scheme as well as the optimized pentadiagonal 4th order Pade Scheme[2]. SSP variant of RK3[30] was used for time discretization at CFL=0.1.

schemes are typically high order and optimized for dispersion characteristics), can be utilized for high-Reynolds number LES. The detrimental effect of dissipative upwind biased discretization on scale-resolving simulations, especially in LES has been well known since late 1990s[156]. In order to gauge the feasibility of such schemes, we consider two non-linear interpolation choices in the context of the WCNS framework introduced earlier: a) WENO-JS [4] (formally 5th order accurate) representing the original WENO-interpolation and b) TENO-8A [84] (formally 8th order accurate) representing the latest class of minimally dissipative non-linear schemes. Figure 1.15 shows the kinetic energy spectrum for decaying homogeneous isotropic turbulence for a sequence of three grid levels (64^3, 128^3 and 256^3) in the $Re_\lambda \rightarrow \infty$ limit. The spectrum makes it clear that the non-dissipative 4th order scheme (with a subgrid scale model) on a 64^3 grid has substantially superior spectral content compared to the 5th order accurate WENO-JS discretization on 256^3 grid. Furthermore, the 64^3 grid 4th order scheme has an effectively equivalent spectral resolution as the 6th order accurate TENO-8A scheme on a 128^3 grid. This is a substantial cost disadvantage for shock-capturing schemes over linear non-dissipative discretization just based on degree-of-freedom requirements, ignoring the substantial computational cost overheards associated with non-linear interpolations

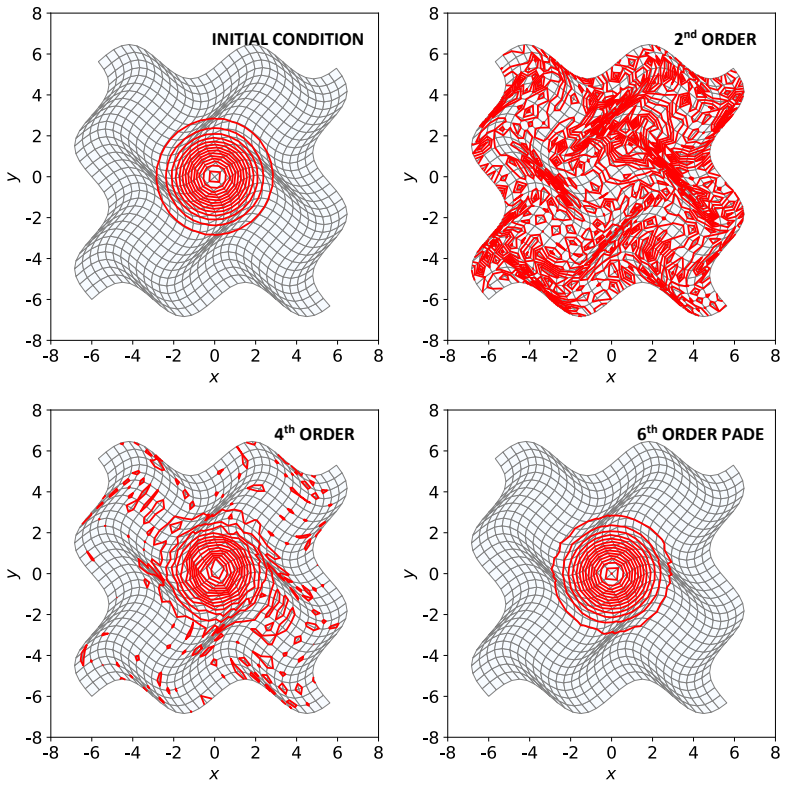

FIGURE 1.14 Same schemes as those shown in Figure 1.13 used to study the inviscid vortex advection problem (defined in [6]) on a wavy mesh. Note that the small-perturbation results in an effectively linearized Euler solution. However, the spatially variable metric terms introduced by the wavy mesh require schemes with superior non-linear stability. All Type-A collocated schemes are unstable for the problem on a wavy grid and require use of de-aliasing filters for stability. All schemes are implemented in their GCL-consistent formulations. Figure generated by Hang Song (Stanford University).

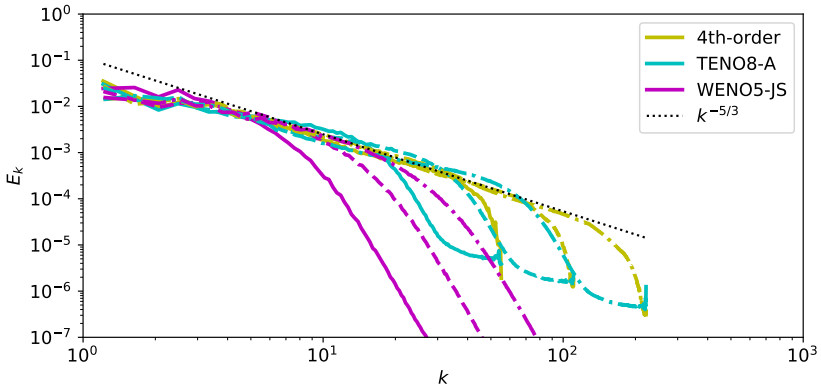

FIGURE 1.15 Kinetic Energy Spectrum for the case introduced in Figure 1.11. Two popular shock-capturing discretizations: a) WENO-5 JS[4], and b) TENO8-A[84] are evaluated without an SGS model (*implicit LES*). They are compared against the fourth order non-dissipative scheme that uses the Vreman SGS model. Solid lines correspond to results on 64^3 grids, dahsed lines correspond to results on 128^3 grids and the dash-dotted lines correspond to results on 128^3 grids. Figure generated by Hang Song (Stanford University).

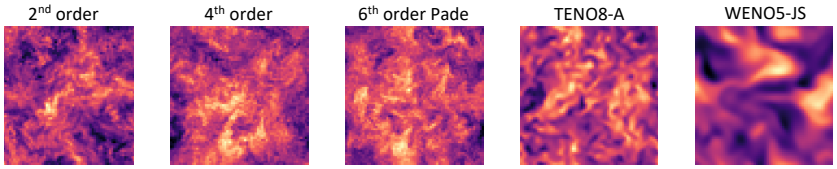

FIGURE 1.16 Instantaneous w-fluctuations for decaying homogeneous isotropic turbulence visualized on an arbitrary XY-plane for 5 schemes at the time corresponding to the spectra shown in Figures 1.11 and 1.15 in a 64^3 domain. Figure generated by Hang Song (Stanford University).

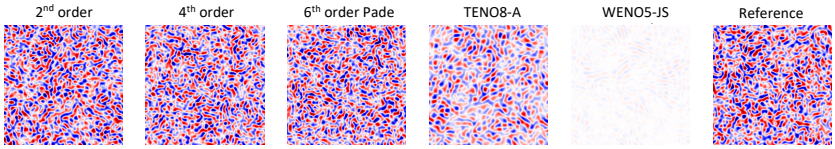

FIGURE 1.17 Band-pass filtered w-fluctuations for the 64^3 simulations compared with those from the reference simulation performed on a 256^3 grid using a 6th order Pade discretization. Spherical spectrally sharp filters are used to isolate content within the $k = 16$ and $k = 32$ spherical shells - this represents the upper half of the resolvable wavenumber range of the 64^3 simulations. Figure generated by Hang Song (Stanford University).

and approximate Riemann solves that linear central schemes do not have.[5] As such while the latest non-linear shock-capture schemes have made substantial progress from the original WENO-JS discretization their suitability for LES is suboptimal based on computational efficiency arguments alone. Other deficiencies such as lack of grid-independent or quantifiable kinetic energy dissipation (as desired in LES) makes them unattractive for LES. Figure 1.16 shows comparisons of instantaneous velocity snapshots for three non-dissipative central discretizations and the two shock capturing schemes in a 64^3 simulation. It is abundantly clear, that even the second order accurate scheme (which also happens to be KEP) provides finer spectral content compared to the minimally dissipative TENO-8A scheme. This observation is reinforced in Figure 1.17 which depicts the band-pass filtered velocity scales present in the upper half of the resolvable wavenumber content in the 64^3 simulations to illustrate the superior spectral properties of the 2nd order scheme compared to either of the two high-order accurate shock-capturing schemes studied. This leads to a very important observation: modified wavenumber analysis (and any optimizations performed using it) does not provide an accurate assessment of a scheme's spectral properties when non-linear processes are dominant; in fact schemes with inferior dispersion characteristics but superior dissipation characteristics (such as the 2nd order central KEP scheme compared with the 6th order TENO-8A scheme) tend to perform better than dissipative schemes with highly optimized dispersion characteristics in LES of high Reynolds number turbulence. This is of particular importance in wall-bounded turbulence which lacks strong inertial instabilities seen in shear-layer turbulence. While second and fourth order discretizations have enjoyed tremendous success in WMLES of high-Reynolds number flows[117–119] using coarse-grids, no such success has been reported using shock-capturing schemes as of the date of this publication.

1.5.3 Blended Schemes

Following the discussion in the previous section regarding unsuitability of shock-capturing schemes for LES, we now discuss the treatments that allow for limiting the scope of such schemes to only regions of the flow where they are needed for robustness. Two main ideas to achieve this are

1. Inviscid flux blending: The midpoint flux is computed as:

$$\boldsymbol{F}_{i+1/2} = (1 - \zeta_{i+1/2})\boldsymbol{F}^{\text{central}}_{i+1/2} + \zeta_{i+1/2}\boldsymbol{F}^{\text{upwind}}_{i+1/2} \tag{1.59}$$

where the $\boldsymbol{F}^{\text{central}}_{i+1/2}$ is a non-dissipatve inviscid flux discretization from any

5. While exact cost comparisons between schemes are difficult due to limited optimization made in academic codes and constantly evolving HPC architectures, some cost assessment was performed in the scheme comparison study of Johnsen et al.[116] who provide evidence that 5th order WENO and 3rd order WENO schemes are approximately 6× and 3× as expensive as a 6th order central scheme respectively based on floating point operations alone.

type-B discretization. It could, for example, be a KEEP flux of arbitrary order of accuracy. $\boldsymbol{F}^{\text{upwind}}_{i+1/2}$ refers to the upwind biased flux computed either using WENO or the WCNS procedure. One disadvantage of this method is its impracticality in generalized curvilinear coordinates since the uni-directional flux blending does not satisfy the geometric conservation constraints needed for free-stream preservation.

2. Variable blending: The left and right biased-interpolated fields (either characteristic or primitive variables) at midpoints are evaluated as

$$\boldsymbol{q}^{L}_{i+1/2} = (1 - \zeta_{i+1/2})\boldsymbol{q}^{C}_{i+1/2} + \zeta_{i+1/2}\boldsymbol{q}^{L}_{i+1/2} \tag{1.60}$$

$$\boldsymbol{q}^{R}_{i+1/2} = (1 - \zeta_{i+1/2})\boldsymbol{q}^{C}_{i+1/2} + \zeta_{i+1/2}\boldsymbol{q}^{R}_{i+1/2} \tag{1.61}$$

where the $\boldsymbol{q}^{L}_{i+1/2}$ and $\boldsymbol{q}^{R}_{i+1/2}$ are the left and right biased variable interpolations respectively, while $\boldsymbol{q}^{C}_{i+1/2}$ is the central interpolation. Note that when $\zeta_{i+1/2} = 0$, $\boldsymbol{q}^{L}_{i+1/2} = \boldsymbol{q}^{R}_{i+1/2} = \boldsymbol{q}^{C}_{i+1/2}$ and a central (non-dissipative) inviscid flux is obtained due to consistency requirements for approximate Riemann solvers. This type of variable blending only works within the WCNS formulation (since it requires the use of a Riemann solver), although it works for generalized curvilinear formulations.

A variety of choices have been utilized in literature for the blending field, $\zeta(\boldsymbol{x}, t)$[107,120–123]. The popular choice reported in literature is the sensor by Ducros et al.[121]:

$$\zeta = \frac{(\nabla \cdot \boldsymbol{u})^2}{(\nabla \cdot \boldsymbol{u})^2 + |\nabla \times \boldsymbol{u}|^2 + \epsilon} \tag{1.62}$$

where ϵ is a small number to prevent division by zero.[6] In low-Mach simulations where dilatation is very low, strain rate magnitude has been introduced to limit the usage of non-dissipative schemes only in regions of the flow dominated by vorticity[124]. An important consequence of the dissipation localization enabled shock sensor is that it allows for utilization of dissipation by computationally inexpensive schemes (such as WENO-JS interpolation with HLL Riemann solver) to generate the upwind flux since one no-longer desires the minimally dissipative attributes from the shock-capturing scheme.

6. It was recently noted by Andy Cook (Lawrence Livermore National lab, private communication, 2022) that the small parameter ϵ in this equations has physical units and the typical value used previously, 10^{-32} (e.g. Kawai, Shankar & Lele[142] and Ghaisas, Subramaniam & Lele[114]) becomes problematic when very large-scale (astrophysical) problems are solved. This prompted Jacob West (Stanford University, 2022) to propose that it be replaced by $\epsilon c^2/\Delta_x^2$ (c being the local sound speed) for dimensional consistency.

1.6 DISCRETIZATION CHALLENGES SPECIFIC TO INCOMPRESSIBLE FLOWS

While the discussion through this point in the Chapter has primarily focused on finite difference discretization for conservation laws involving hyperbolic PDEs (compressible Navier-Stokes), additional significant challenges are posed by elliptic PDEs, such as the incompressible Navier-Stokes equations. While the reader is referred to Chapter 11 for a detailed review of challenges posed by the spatial non-locality of pressure due to the incompressible flow assumption, here we briefly discuss some attributes specific to finite difference discretizations.

Incompressible finite difference formulations of Navier-Stokes for scale resolving simulations have traditionally been implemented via a projection method [25,26] (as opposed to other methods such as artificial compressibility method commonly used in steady-state solvers [27]) requiring an elliptic linear solve of the Poisson equation. Typically, enforcing surface velocity boundary condition requires solution to a Neumann problem (homogeneous for inviscid boundary conditions, and inhomogeneous for viscous boundary conditions). To facilitate a concise discussion of several discretization considerations, the periodic domain problem is considered in the following; the discussion can be extended to the homogeneous Neumann boundary problem in Cartesian formulations via use of cosine transforms instead of Fourier transform used for the analysis of the periodic problem as discussed later in the section,

$$\nabla \cdot (\nabla \phi) = \nabla \cdot \boldsymbol{u}^{\star} \;\; ; \;\; \boldsymbol{u}^{n+1} = \boldsymbol{u}^{\star} - \nabla \phi \tag{1.63}$$

Note that the variable, $\boldsymbol{u}^{\star}$ is commonly referred to as an *intermediate velocity* which is computed after the advective time-advancement step (using a standard time-stepping scheme such as a RK4 substep or a combination of explicit and implicit schemes for inviscid and viscous fluxes respectively) which is not discretely divergence free. Hence a projection operation is required prior to obtaining the solution, $\boldsymbol{u}^{n+1}$ at the next timestep. Such a projection can be written concisely in Fourier space as:

$$\hat{u}_i^{n+1}(\boldsymbol{k}) = \left(\delta_{ij} - \frac{\tilde{k}_i \tilde{k}_j}{\overline{k}^2}\right) \hat{u}_j^{\star}(\boldsymbol{k}) \implies \hat{\boldsymbol{u}}^{n+1}(\boldsymbol{k}) = \boldsymbol{\mathcal{P}}(\tilde{\boldsymbol{k}}, \overline{\boldsymbol{k}}^{\boldsymbol{2}}) \hat{\boldsymbol{u}}^{\star}(\boldsymbol{k}) \tag{1.64}$$

where, $\tilde{k}_i$ is the modified wavenumber for the discrete first-derivative operator (assumed to be identical for the gradient and divergence operators) seen on the right-hand-side of Equation 1.63), $\overline{k}^2$ is the discrete Laplacian operator seen in the left hand side of Poisson equation for the scalar field, ϕ in Equation 1.63. The tensor projection operator, $\boldsymbol{\mathcal{P}}$ for a given Fourier mode at wavenumber, k is thus a function of both the first derivative discrete operator, $\tilde{k}$ and the second derivative operator used in the Laplacian kernel, $\overline{k}^2$. At this point, it is clear that the choice of using $(\partial/\partial_x) \times (\partial/\partial_x)$ for the Laplacian operator $(\overline{k}^2)$ is not

permissible since the projection kernel, $\mathcal{P}$ is singular at the Nyquist wavenumber $k = \pi$ (see the middle pane of Figure 1.6). However, both the staggered and the direct operators are candidates for the Laplacian operator since they do not suffer from this Nyquist singularity[7]. To understand this projection error for the various choices, consider the post-projection discrete divergence error:

$$\tilde{k}_i \hat{u}_i^{n+1} = \tilde{k}_i \mathcal{P}_{ij} \hat{u}_j^{\star} = \left(\delta_{ij} - \frac{\tilde{k}_i \tilde{k}_j}{\overline{k}^2} \right) \tilde{k}_i u_j^{\star} = \mathcal{E}(\tilde{k}, \overline{k}^2) \tilde{k}_j u_j^{\star} \tag{1.65}$$

which involves the scalar projection error $\mathcal{E}(\tilde{k}, \overline{k}^2)$ in the available choices for the divergence and gradient operators ($\tilde{k}$) and the (direct) Laplacian operator ($\overline{k}^2$). Use of the discrete second derivative appears to be particularly attractive : (1) the stencil size is smaller (schemes higher than second order accurate) compared to consistent formulation ($\mathcal{E}(\tilde{k}, \overline{k}^2) = 0$) using two staggered first derivatives ($\overline{k}^2 = \tilde{k}_m \tilde{k}_m$), and (2) the linear system is more diagonally dominant and as such more attractive for iterative solvers. For (implicit) finite difference schemes such as Pade-schemes the consistent Laplacian operator ($\overline{k}^2 = \tilde{k}_m \tilde{k}_m$) is not a sparse operator. Such (inconsistent) formulations utilizing the second derivative operators have been used in literature (especially for DNS [127]). However, as shown in Figure 1.18 the spectral representation of the resulting projection errors makes this strategy unappealing for LES.

1. Collocated grid storage pattern necessitates use of collocated first derivative operators for gradient and divergence, which results in complete decoupling ($\mathcal{E} = 1$) between the correction $\nabla\phi$ and the intermediate velocity, $\boldsymbol{u}^{\star}$ at the Nyquist wavenumber. This is often referred to as *pressure-velocity decoupling* or *checkerboarding* which contaminates solutions for high-Reynolds flows.
2. On staggered grids, which utilize staggered divergence and gradient operators, this decoupling does not occur. However, errors due to inconsistent Laplacian operators result in projection errors at high-wavenumbers. These wavenumbers promote numerical instability due to loss of discrete mass-conservation. Furthermore, it is important to note that these errors are larger for higher-order schemes. Consistent Laplacian operators should be used particularly in LES of high Reynolds number flows using high order accurate discretizations for inviscid fluxes.

One solution to address the non-sparse character of the consistent Laplacian operator for Pade schemes is to utilize direct solvers in Fourier space[28,29]. Exact projection can be achieved via utilizing modified wavenumbers for the staggered Pade operators and cosine transforms are utilized for homogeneous

7. The singularity of the projection kernel at $k = 0$ exists for all operators, due to the ill-posedness of the Neumann and/or the periodic Poisson equation. This is not particularly pertinent in the present discussion since the domain averaged value ($\boldsymbol{k} = 0$) does not play any role.

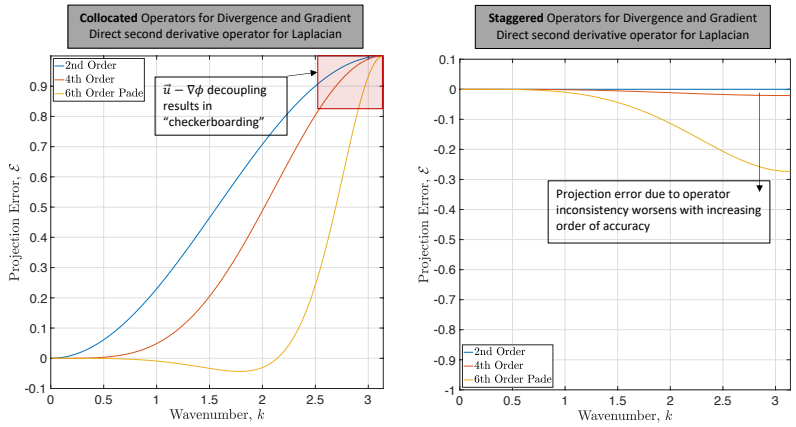

FIGURE 1.18 Spectral representation of projection errors when inconsistent definitions are used for the Laplacian operator and the first derivative (divergence and gradient) operators. For consistent Laplacian operators ($\bar{k}^2 = \tilde{k}_j \tilde{k}_j$) this projection error is exactly zero regardless of the accuracy of the scheme. The second order explicit schemes have the $\mathcal{E}(k) = 0$ property since stencil for a direct second derivative operator is identical to the stencil obtained for consecutive application of two staggered first derivative operators.

Neumann boundary conditions.

1.7 ADDITIONAL CONSIDERATIONS

1.7.1 Boundary Treatments

A comprehensive summary of boundary conditions applicable to compressible flow simulations has been provided by Colonius[131], and is also covered within Chapter 8. Boundary conditions for compressible Navier-Stokes simulation leverage the hyperbolic character of the governing equations and ideas based on characteristic decomposition provide an elegant treatment to ensure solution global accuracy and avoid ill-posedness due to over- or under-prescription [132,133]. Ghost-cell based finite difference schemes for enforcing characteristic boundary conditions were presented recently by Motheau et al.[171]. In incompressible flows, the pressure-field plays a major role in enforcing any Dirichlet boundary conditions for velocity via the solution to the inhomogeneous Poisson equation. The reader is referred to the work by Gresho & Sani for a detailed discussion on pressure boundary conditions applicable for incompressible flows. Turbulence-resolving simulations of wall-bounded flows require some additional considerations. Spurious acoustic reflections from solid walls can particularly be detrimental, and Tam & Dong [172] have developed ghost-cell based boundary schemes that minimize such spurious modes typically present in high order finite difference schemes (such as the DRP scheme). In spatially evolving boundary

layers, one seeks to develop a fully turbulent state at the shortest possible distance from the inflow, and the reader is referred to the review by Wu[134] for a discussion of recycling methods [135] (also applicable to engineering compressible flows[136] as well environmental incompressible flows[137]) and a host of synthetic inflow generation methods applicable in DNS, LES (wall-modelled or resolved) and hybrid RANS/LES. In the context of boundary closures for finite difference discretizations, methods utilizing sided stencils (as opposed to ghost cells) have historically been more popular. For higher order schemes, the formal order of accuracy of the interior scheme can only be retained if the boundary scheme is at most one order less than the interior scheme[161]. To study linear stability in semi-infinite or finite domains for initial boundary value problems normal mode analysis[162–164] (often referred to as G-K-S theory) in terms of generalized eigenvalues is typically used. Trefethen[165] later presented an elegant analogy between stability based on eigenvalues and the group velocity of the boundary scheme - carrying the energy either in or out of the domain. Since application of G-K-S theory in multi-stage time discretization schemes (such as RK schemes) is analytically tedious (if not insurmountable), Strikwerda's [166] result showing that the semi-discrete (space discretized, time continuous as in method-of-lines approach) analysis can be used to obtain the necessary and sufficient conditions for the stability of the fully discrete system (if advanced using a locally stable temporal scheme), extended the scope of G-K-S based stability analysis to higher order spatio-temporal finite difference discretizations. Carpenter, Gottlieb & Abarbanel[167] subsequently performed G-K-S analysis of higher order finite difference schemes including Pade Schemes and argued that a more nuanced definition of stability, referred to as *asymptotic stability* (based on solution boundedness) was needed for use of such schemes in practical simulations, and the authors proposed new boundary closures for both 4th and 6th order Pade interior schemes that were asymptotically stable. However, these schemes were found to be time-divergent when used in a system of coupled ODEs, and the authors subsequently proposed a new procedure relying on derivative approximations of implicit compact scheme with Strand's[59] summation-by-parts property along with a new procedure referred to as *Simultaneous Approximation Terms* (SAT) to construct schemes that were truly asymptotically stable (time-stable)[168]. Nordstrom & Carpenter[160] later generalized the results for Euler and Navier-Stokes equations along with applications to interface conditions such as those that occur at coarse-fine grid boundaries on octree-grids discussed previously. Svard et al. [169,170] have more recently extended the formulation further for dealing with viscous no-slip boundaries as well as for non-reflective far field boundaries.

1.7.2 Time Integration

Since convective fluxes are dominant in scale-resolving simulations of turbulence, explicit time-integration based on method-of-lines procedure using multi-

stage Runge-Kutta schemes[128] is by far the most popular discretization choice for LES. Some of this is influenced by the work by Choi & Moin[129] who studied the filtering effect of implicit time-stepping schemes for wall-bounded flows and demonstrated that wall-turbulence could not be sustained if the time-step size exceeded the turn-over timescales of the smallest spatially resolved eddies, which in their wall-resolved case corresponded to the Kolmogorov scale. In wall-modelled LES, since the grid aspect ratios are ($O(1)$), implicit time-stepping does not offer any particular advantage in regards to computational efficiency since one expects to resolve temporal motions corresponding to the grid Nyquist wavenumbers - and stability limitations of explicit time-stepping schemes (based on CFL) provide an appropriate bound. However, when compressible-flow equations are solved in low-Mach regimes, the additional temporal stiffness associated with acoustics can be mitigated using implicit time-stepping. Furthermore, in the case of either wall-resolved LES or hybrid RANS/LES, the viscous diffusion scaling ($\Delta_t \propto \Delta_x^2$) necessitates the use of implicit time-stepping schemes for at least the viscous terms[26]. In applications involving multi-physics and extreme flow conditions, the SSP/TVD RK schemes developed by Gottlieb et al.[30] have gained popularity in the past two decades. The key strength of such discretizations is the property that given a stable (defined using an appropriate *total variation* norm) semi-discretization of a conservation law under a first-order Euler forward time-stepping scheme, the multi-stage RK scheme (typically designed as a convex combination of multiple forward Euler steps) will maintain the stability in the same total variation norm; this is particularly useful for spatial discretization schemes designed to meet specific positivity-preserving properties, since these multi-stage RK schemes inherit those positivity preserving properties while offering higher-order accuracy. Finally, the reader is referred to the work by Bernardini & Pirozzoli[130] who provide a general framework for optimizing RK schemes in regards to computational cost and error specifically targeting computational aeroacoustics applications; while these schemes are demonstrably advantageous for wave-propagation problems, their advantages in LES of turbulence dominated phenomena remain to be established.

1.7.3 Additional Topics

Space limitations do not allow a discussion on alternative approaches to achieve robust finite difference approximations, such as the Summation by Parts (SBP) operators[59,152,153], details regarding robust treatment of near-boundary discretization and boundary conditions, and the diffuse interface treatment for multiphase and multimaterial flows[154,155]. Furthermore, several computational considerations regarding implementation of finite difference schemes on modern accelerators such as Graphical Processing Units (GPUs) were not discussed - the reader is referred to external references that focus on this specific topic, especially those in the context of implicit operators[176–178].

1.8 SUMMARIZING REMARKS

Several characteristics of finite difference discretization were discussed in the context of scale-resolving turbulence simulations. Three key takeaways are summarized as follows:

1. The choice of an appropriate finite difference scheme is problem dependent. There is no single scheme that is optimal for any arbitrary flow-scenario:
   - **a.** Dispersion error optimized schemes are excellent for linear phenomena such as instabilities (in their linear regime) or wave-propagation but cannot capture shocks and contact discontinuities. While their low-dispersion errors enable more accurate representation of phase information (important for problems with sharp interfaces), these methods are also computationally more expensive. Non-dissipative lower order (such as second order) discretizations may offer effectively same spectral resolution when non-linear processes dominate. However, since most applications involve some mean convection (linear-process), higher order non-dissipative discretizations may still be useful for LES based on accuracy-per-unit computational cost based trade-offs. The fourth order scheme discussed in the chapter that utilizes both midpoint and nodal inviscid fluxes is one such option since it requires the same stencil size as a second order finite difference discretization of the viscous terms.
   - **b.** Kinetic energy and entropy preserving schemes are very attractive in high Reynolds number LES due to their superior non-linear robustness and easy extensions to obtain high-order accuracy or dispersion error optimization. However, they cannot capture shocks or contact discontinuities, and most practical applications utilizing their high-order accurate variants still rely on some form of dealiasing - such as stencil based low-pass filtering of the solution.
   - **c.** Non-linear shock-capturing schemes can offer exceptional robustness in extreme flow-conditions, however even the latest so-called *minimally dissipative* formulations pale in comparison to the spectral resolution offered by non-dissipative central formulations (including second order accurate schemes) in flows dominated by non-linear transport processes such as turbulence at high-Reynolds numbers.
   - **d.** Sensor-based blending between central and upwind-biased schemes in extreme flow configurations, and/or artificial dissipation in less-extreme flow configurations can potentially serve as the most pragmatic solution to address a wide range of flow configurations.
2. Finite difference schemes using structured curvilinear overset as well as cartesian octree grid topologies have enjoyed tremendous success in scale resolving simulations in highly complex, non-canonical flows. Grid generation and satisfaction of additional geometric constraints are the major challenges for curvilinear formulations, while numerical treatment for coarse-fine interfaces and immersed boundary description of geometries are the primary

challenges in cartesian octree formulations.

3. Non-linear stability and robustness is of critical importance in turbulence simulations. Staggered variable placement is more naturally suited for lowering aliasing errors in non-linear fluxes. Staggering also offers superior properties over collocated storage schemes for elliptic solves required for incompressible and Low-Mach number conditions. However, even in collocated variable schemes, careful discretization of both inviscid and viscous fluxes utilizing nodal midpoints and appropriate interpolation and derivative operations can achieve a very high degree of robustness.

[1] Tam, C. & Webb, J. Dispersion-relation-preserving finite difference schemes for computational acoustics. *Journal Of Computational Physics*. **107**, 262-281 (1993)

[2] Lele, S. Compact finite difference schemes with spectral-like resolution. *Journal Of Computational Physics*. **103**, 16-42 (1992)

[3] Deng, X. & Zhang, H. Developing high-order weighted compact nonlinear schemes. *Journal Of Computational Physics*. **165**, 22-44 (2000)

[4] Jiang, G. & Shu, C. Efficient implementation of weighted ENO schemes. *Journal Of Computational Physics*. **126**, 202-228 (1996)

[5] Bogey, C. & Bailly, C. A family of low dispersive and low dissipative explicit schemes for flow and noise computations. *Journal Of Computational Physics*. **194**, 194-214 (2004)

[6] Visbal, M. & Gaitonde, D. On the use of higher-order finite-difference schemes on curvilinear and deforming meshes. *Journal Of Computational Physics*. **181**, 155-185 (2002)

[7] Steger, J. Implicit finite-difference simulation of flow about arbitrary two-dimensional geometries. *AIAA Journal*. **16**, 679-686 (1978)

[8] Pulliam, T. & Steger, J. Implicit finite-difference simulations of three-dimensional compressible flow. *AIAA Journal*. **18**, 159-167 (1980)

[9] Thomas, P. & Lombard, C. Geometric conservation law and its application to flow computations on moving grids. *AIAA Journal*. **17**, 1030-1037 (1979)

[10] Nonomura, T., Iizuka, N. & Fujii, K. Freestream and vortex preservation properties of high-order WENO and WCNS on curvilinear grids. *Computers & Fluids*. **39**, 197-214 (2010)

[11] Song, H., Ghate, A., Matsuno, K., West, J., Subramaniam, A., Brown, L. & Lele, S. Robust high-resolution simulations of compressible turbulent flows without filtering. *AIAA AVIATION 2022 Forum*. pp. 4122 (2022)

[12] Song, H., Matsuno, K., West, J., Subramaniam, A., Ghate, A. & Lele, S. Scalable Parallel Linear Solver for Compact Banded Systems on Heterogeneous Architectures. *Journal Of Computational Physics*. pp. 111443 (2022)

[13] Shukla, R. & Zhong, X. Derivation of high-order compact finite difference schemes for non-uniform grid using polynomial interpolation. *Journal Of Computational Physics*. **204**, 404-429 (2005)

[14] Gamet, L., Ducros, F., Nicoud, F. & Poinsot, T. Compact finite difference schemes on non-uniform meshes. Application to direct numerical simulations of compressible flows. *International Journal For Numerical Methods In Fluids*. **29**, 159-191 (1999)

[15] You, D., Mittal, R., Wang, M. & Moin, P. Analysis of stability and accuracy of finite-difference schemes on a skewed mesh. *Journal Of Computational Physics*. **213**, 184-204 (2006)

[16] Teyssier, R. Cosmological hydrodynamics with adaptive mesh refinement-A new high resolution code called RAMSES. *Astronomy & Astrophysics*. **385**, 337-364 (2002)

[17] Almgren, A., Beckner, V., Bell, J., Day, M., Howell, L., Joggerst, C., Lijewski, M., Nonaka, A., Singer, M. & Zingale, M. CASTRO: A new compressible astrophysical solver. I. Hydrodynamics and self-gravity. *The Astrophysical Journal*. **715**, 1221 (2010)

[18] Peron, S. & Benoit, C. Automatic off-body overset adaptive Cartesian mesh method based on an octree approach. *Journal Of Computational Physics*. **232**, 153-173 (2013)

[19] Berger, M. & Oliger, J. Adaptive mesh refinement for hyperbolic partial differential equations. *Journal Of Computational Physics*. **53**, 484-512 (1984)

[20] Nonomura, T. & Fujii, K. Robust explicit formulation of weighted compact nonlinear scheme. *Computers & Fluids*. **85** pp. 8-18 (2013)

[21] Sjögreen, B. & Yee, H. Multiresolution wavelet based adaptive numerical dissipation control for high order methods. *Journal Of Scientific Computing*. **20**, 211-255 (2004)

[22] Pantano, C., Deiterding, R., Hill, D. & Pullin, D. A low numerical dissipation patch-based

adaptive mesh refinement method for large-eddy simulation of compressible flows. *Journal Of Computational Physics*. **221**, 63-87 (2007)

[23] Almgren, A., Bell, J., Colella, P., Howell, L. & Welcome, M. A conservative adaptive projection method for the variable density incompressible Navier–Stokes equations. *Journal Of Computational Physics*. **142**, 1-46 (1998)

[24] McCormick, S. & Thomas, J. The fast adaptive composite grid (FAC) method for elliptic equations. *Mathematics Of Computation*. **46**, 439-456 (1986)

[25] Chorin, A. The numerical solution of the Navier-Stokes equations for an incompressible fluid. *Bulletin Of The American Mathematical Society*. **73**, 928-931 (1967)

[26] Kim, J. & Moin, P. Application of a fractional-step method to incompressible Navier-Stokes equations. *Journal Of Computational Physics*. **59**, 308-323 (1985)

[27] Ferziger, J., Perić, M. & Street, R. Computational methods for fluid dynamics. (Springer,2002)

[28] Laizet, S. & Lamballais, E. High-order compact schemes for incompressible flows: A simple and efficient method with quasi-spectral accuracy. *Journal Of Computational Physics*. **228**, 5989-6015 (2009)

[29] Ghate, A. & Lele, S. K. Subfilter-scale enrichment of planetary boundary layer large eddy simulation using discrete Fourier–Gabor modes. *Journal Of Fluid Mechanics*. **819** pp. 494-539 (2017)

[30] Gottlieb, S., Shu, C. & Tadmor, E. Strong stability-preserving high-order time discretization methods. *SIAM Review*. **43**, 89-112 (2001)

[31] Sengupta, T., Sircar, S. & Dipankar, A. High accuracy schemes for DNS and acoustics. *Journal Of Scientific Computing*. **26**, 151-193 (2006)

[32] Lele, S. Computational aeroacoustics-A review. *35th Aerospace Sciences Meeting And Exhibit*. pp. 18 (1997)

[33] Tam, C. Computational aeroacoustics: An overview of computational challenges and applications. *International Journal Of Computational Fluid Dynamics*. **18**, 547-567 (2004)

[34] Uzun, A. & Malik, M. High-Fidelity Simulation of Turbulent Flow Past Gaussian Bump. *AIAA Journal*. pp. 1-20 (2021)

[35] Livescu, D. & Ristorcelli, J. Buoyancy-driven variable-density turbulence. *Journal Of Fluid Mechanics*. **591** pp. 43-71 (2007)

[36] Maeder, T., Adams, N. & Kleiser, L. Direct simulation of turbulent supersonic boundary layers by an extended temporal approach. *Journal Of Fluid Mechanics*. **429** pp. 187-216 (2001)

[37] Pantano, C. & Sarkar, S. A study of compressibility effects in the high-speed turbulent shear layer using direct simulation. *Journal Of Fluid Mechanics*. **451** pp. 329-371 (2002)

[38] Hill, D., Pantano, C. & Pullin, D. Large-eddy simulation and multiscale modelling of a Richtmyer–Meshkov instability with reshock. *Journal Of Fluid Mechanics*. **557** pp. 29-61 (2006)

[39] Tritschler, V., Olson, B., Lele, S., Hickel, S., Hu, X. & Adams, N. On the Richtmyer–Meshkov instability evolving from a deterministic multimode planar interface. *Journal Of Fluid Mechanics*. **755** pp. 429-462 (2014)

[40] Armenio, V. & Sarkar, S. An investigation of stably stratified turbulent channel flow using large-eddy simulation. *Journal Of Fluid Mechanics*. **459** pp. 1-42 (2002)

[41] Porté-Agel, F., Meneveau, C. & Parlange, M. A scale-dependent dynamic model for large-eddy simulation: application to a neutral atmospheric boundary layer. *Journal Of Fluid Mechanics*. **415** pp. 261-284 (2000)

[42] Nicoud, F., Toda, H., Cabrit, O., Bose, S. & Lee, J. Using singular values to build a subgrid-scale model for large eddy simulations. *Physics Of Fluids*. **23**, 085106 (2011)

[43] Moin, P. & Verzicco, R. On the suitability of second-order accurate discretizations for turbulent

flow simulations. *European Journal Of Mechanics-B/Fluids*. **55** pp. 242-245 (2016)

[44] Stich, G., Ghate, A., Housman, J. & Kiris, C. Wall Modeled Large Eddy Simulations for NASA's jet noise consensus database of single-stream, round, convergent jets.. *AIAA SCITECH 2022 Forum*. pp. 0684 (2022)

[45] Vreman, A. An eddy-viscosity subgrid-scale model for turbulent shear flow: Algebraic theory and applications. *Physics Of Fluids*. **16**, 3670-3681 (2004)

[46] Rosales, C. & Meneveau, C. Linear forcing in numerical simulations of isotropic turbulence: Physical space implementations and convergence properties. *Physics Of Fluids*. **17**, 095106 (2005)

[47] Kuya, Y. & Kawai, S. High-order accurate kinetic-energy and entropy preserving (KEEP) schemes on curvilinear grids. *Journal Of Computational Physics*. **442** pp. 110482 (2021)

[48] Feiereisen, W. Numerical simulation of a compressible, homogeneous, turbulent shear flow. (Stanford University,1981)

[49] LeVeque, R. & Leveque, R. Numerical methods for conservation laws. (Springer,1992)

[50] Lax, P. Hyperbolic systems of conservation laws and the mathematical theory of shock waves. (SIAM,1973)

[51] Harten, A. On the symmetric form of systems of conservation laws with entropy. *Journal Of Computational Physics*. **49** (1983)

[52] Pirozzoli, S. Numerical methods for high-speed flows. *Annual Review Of Fluid Mechanics*. **43** pp. 163-194 (2011)

[53] Blaisdell, G., Spyropoulos, E. & Qin, J. The effect of the formulation of nonlinear terms on aliasing errors in spectral methods. *Applied Numerical Mathematics*. **21**, 207-219 (1996)

[54] Kennedy, C. & Gruber, A. Reduced aliasing formulations of the convective terms within the Navier–Stokes equations for a compressible fluid. *Journal Of Computational Physics*. **227**, 1676-1700 (2008)

[55] Jameson, A. Formulation of kinetic energy preserving conservative schemes for gas dynamics and direct numerical simulation of one-dimensional viscous compressible flow in a shock tube using entropy and kinetic energy preserving schemes. *Journal Of Scientific Computing*. **34**, 188-208 (2008)

[56] Honein, A. & Moin, P. Higher entropy conservation and numerical stability of compressible turbulence simulations. *Journal Of Computational Physics*. **201**, 531-545 (2004)

[57] Kuya, Y., Totani, K. & Kawai, S. Kinetic energy and entropy preserving schemes for compressible flows by split convective forms. *Journal Of Computational Physics*. **375** pp. 823-853 (2018)

[58] Kok, J. A high-order low-dispersion symmetry-preserving finite-volume method for compressible flow on curvilinear grids. *Journal Of Computational Physics*. **228**, 6811-6832 (2009)

[59] Strand, B. Summation by parts for finite difference approximations for d/dx. *Journal Of Computational Physics*. **110**, 47-67 (1994)

[60] Morinishi, Y. Skew-symmetric form of convective terms and fully conservative finite difference schemes for variable density low-Mach number flows. *Journal Of Computational Physics*. **229**, 276-300 (2010)

[61] Shima, N., Kuya, Y., Tamaki, Y. & Kawai, S. Preventing spurious pressure oscillations in split convective form discretization for compressible flows. *Journal Of Computational Physics*. **427** pp. 110060 (2021)

[62] Lax, P. Systems of conservation laws. (LOS ALAMOS NATIONAL LAB NM,1959)

[63] Pirozzoli, S. Generalized conservative approximations of split convective derivative operators. *Journal Of Computational Physics*. **229**, 7180-7190 (2010)

[64] Ducros, F., Laporte, F., Soulères, T., Guinot, V., Moinat, P. & Caruelle, B. High-order fluxes for

conservative skew-symmetric-like schemes in structured meshes: application to compressible flows. *Journal Of Computational Physics*. **161**, 114-139 (2000)

[65] Asada, H. & Kawai, S. LES of full aircraft configuration using non-dissipative KEEP scheme with conservative explicit filter. *AIAA SCITECH 2022 Forum*. pp. 0449 (2022)

[66] Godunov, S. A difference scheme for numerical solution of discontinuous solution of hydrodynamic equations. *Math. Sbornik*. **47** pp. 271-306 (1959)

[67] Harten, A. High resolution schemes for hyperbolic conservation laws. *Journal Of Computational Physics*. **135**, 260-278 (1997)

[68] Harten, A. ENO schemes with subcell resolution. *Journal Of Computational Physics*. **83**, 148-184 (1989)

[69] Yee, H. A class of high-resolution explicit and implicit shock-capturing methods. (1989)

[70] Harten, A., Hyman, J., Lax, P. & Keyfitz, B. On finite-difference approximations and entropy conditions for shocks. *Communications On Pure And Applied Mathematics*. **29**, 297-322 (1976)

[71] Garnier, E., Mossi, M., Sagaut, P., Comte, P. & Deville, M. On the use of shock-capturing schemes for large-eddy simulation. *Journal Of Computational Physics*. **153**, 273-311 (1999)

[72] Larsson, J., Lele, S. & Moin, P. Effect of numerical dissipation on the predicted spectra for compressible turbulence. *Annual Research Briefs*. pp. 47-57 (2007)

[73] Pirozzoli, S. On the spectral properties of shock-capturing schemes. *Journal Of Computational Physics*. **219**, 489-497 (2006)

[74] Fu, L., Hu, X. & Adams, N. A targeted ENO scheme as implicit model for turbulent and genuine subgrid scales. *Communications In Computational Physics*. **26**, 311-345 (2019)

[75] Wong, M., Angel, J., Barad, M. & Kiris, C. A positivity-preserving high-order weighted compact nonlinear scheme for compressible gas-liquid flows. *Journal Of Computational Physics*. **444** pp. 110569 (2021)

[76] Kawai, S. & Lele, S. Localized artificial diffusivity scheme for discontinuity capturing on curvilinear meshes. *Journal Of Computational Physics*. **227**, 9498-9526 (2008)

[77] Subramaniam, A. & Lele, S. Numerical simulation of multi-material mixing in an inclined interface Richtmyer-Meshkov instability. *AIP Conference Proceedings*. **1793**, 150006 (2017)

[78] Kiris, C., Ghate, A., Duensing, J., Browne, O., Housman, J., Stich, G., Kenway, G., Dos Santos Fernandes, L. & Machado, L. High-Lift Common Research Model: RANS, HRLES, and WMLES perspectives for CLmax prediction using LAVA. *AIAA SCITECH 2022 Forum*. pp. 1554 (2022)

[79] Ghate, A., Kenway, G., Stich, G. & Kiris, C. Wall-modelled Large Eddy Simulations of High-Lift CRM using Curvilinear and Cartesian immersed boundary formulations. *AIAA AVIATION 2022 Forum*. pp. 1554 (2022)

[80] Sandham, N., Li, Q. & Yee, H. Entropy splitting for high-order numerical simulation of compressible turbulence. *Journal Of Computational Physics*. **178**, 307-322 (2002)

[81] Sandham, N., Yao, Y. & Lawal, A. Large-eddy simulation of transonic turbulent flow over a bump. *International Journal Of Heat And Fluid Flow*. **24**, 584-595 (2003)

[82] Cook, A. & Cabot, W. Hyperviscosity for shock-turbulence interactions. *Journal Of Computational Physics*. **203**, 379-385 (2005)

[83] Cook, A. Artificial fluid properties for large-eddy simulation of compressible turbulent mixing. *Physics Of Fluids*. **19**, 055103 (2007)

[84] Fu, L. A very-high-order TENO scheme for all-speed gas dynamics and turbulence. *Computer Physics Communications*. **244** pp. 117-131 (2019)

[85] Brès, G., Jordan, P., Jaunet, V., Le Rallic, M., Cavalieri, A., Towne, A., Lele, S., Colonius, T. & Schmidt, O. Importance of the nozzle-exit boundary-layer state in subsonic turbulent jets. *Journal Of Fluid Mechanics*. **851** pp. 83-124 (2018)

[86] Donzis, D. & Jagannathan, S. Fluctuations of thermodynamic variables in stationary compressible turbulence. *Journal Of Fluid Mechanics*. **733** pp. 221-244 (2013)

[87] Matsuno, K. & Lele, S. Internal regulation in compressible turbulent shear layers. *Journal Of Fluid Mechanics*. **907** (2021)

[88] Wong, M., Livescu, D. & Lele, S. High-resolution Navier-Stokes simulations of Richtmyer-Meshkov instability with reshock. *Physical Review Fluids*. **4**, 104609 (2019)

[89] Larsson, J., Bermejo-Moreno, I. & Lele, S. Reynolds-and Mach-number effects in canonical shock–turbulence interaction. *Journal Of Fluid Mechanics*. **717** pp. 293-321 (2013)

[90] Bermejo-Moreno, I., Campo, L., Larsson, J., Bodart, J., Helmer, D. & Eaton, J. Confinement effects in shock wave/turbulent boundary layer interactions through wall-modelled large-eddy simulations. *Journal Of Fluid Mechanics*. **758** pp. 5-62 (2014)

[91] Pirozzoli, S., Grasso, F. & Gatski, T. Direct numerical simulation and analysis of a spatially evolving supersonic turbulent boundary layer at M= 2.25. *Physics Of Fluids*. **16**, 530-545 (2004)

[92] Ghate, A., Kenway, G., Stich, G., Browne, O., Housman, J. & Kiris, C. Transonic lift and drag predictions using wall-modelled large eddy simulations. *AIAA Scitech 2021 Forum*. pp. 1439 (2021)

[93] Roe, P. Approximate Riemann solvers, parameter vectors, and difference schemes. *Journal Of Computational Physics*. **43**, 357-372 (1981)

[94] Toro, E., Spruce, M. & Speares, W. Restoration of the contact surface in the HLL-Riemann solver. *Shock Waves*. **4**, 25-34 (1994)

[95] Liou, M. & Steffen Jr, C. A new flux splitting scheme. *Journal Of Computational Physics*. **107**, 23-39 (1993)

[96] Nonomura, T. & Fujii, K. Effects of difference scheme type in high-order weighted compact nonlinear schemes. *Journal Of Computational Physics*. **228**, 3533-3539 (2009)

[97] Hu, X., Wang, Q. & Adams, N. An adaptive central-upwind weighted essentially non-oscillatory scheme. *Journal Of Computational Physics*. **229**, 8952-8965 (2010)

[98] Borges, R., Carmona, M., Costa, B. & Don, W. An improved weighted essentially non-oscillatory scheme for hyperbolic conservation laws. *Journal Of Computational Physics*. **227**, 3191-3211 (2008)

[99] Fu, L., Hu, X. & Adams, N. A family of high-order targeted ENO schemes for compressible-fluid simulations. *Journal Of Computational Physics*. **305** pp. 333-359 (2016)

[100] Subramaniam, A., Wong, M. & Lele, S. A high-order weighted compact high resolution scheme with boundary closures for compressible turbulent flows with shocks. *Journal Of Computational Physics*. **397** pp. 108822 (2019)

[101] Zhang, H., Xu, C. & Dong, H. An extended seventh-order compact nonlinear scheme with positivity-preserving property. *Computers & Fluids*. **229** pp. 105085 (2021)

[102] Tang, L., Song, S. & Zhang, H. High-order maximum-principle-preserving and positivity-preserving weighted compact nonlinear schemes for hyperbolic conservation laws. *Applied Mathematics And Mechanics*. **41**, 173-192 (2020)

[103] Hu, X., Adams, N. & Shu, C. Positivity-preserving method for high-order conservative schemes solving compressible Euler equations. *Journal Of Computational Physics*. **242** pp. 169-180 (2013)

[104] Zhang, X. & Shu, C. Positivity-preserving high order finite difference WENO schemes for compressible Euler equations. *Journal Of Computational Physics*. **231**, 2245-2258 (2012)

[105] Lamballais, E., Fortuné, V. & Laizet, S. Straightforward high-order numerical dissipation via the viscous term for direct and large eddy simulation. *Journal Of Computational Physics*. **230**, 3270-3275 (2011)

[106] VonNeumann, J. & Richtmyer, R. A method for the numerical calculation of hydrodynamic shocks. *Journal Of Applied Physics*. **21**, 232-237 (1950)

[107] Jameson, A., Schmidt, W. & Turkel, E. Numerical solution of the Euler equations by finite volume methods using Runge Kutta time stepping schemes. *14th Fluid And Plasma Dynamics Conference*. pp. 1259 (1981)

[108] Pulliam, T. High order accurate finite-difference methods: as seen in OVERFLOW. *20th AIAA Computational Fluid Dynamics Conference*. pp. 3851 (2011)

[109] Brehm, C., Barad, M., Housman, J. & Kiris, C. A comparison of higher-order finite-difference shock capturing schemes. *Computers & Fluids*. **122** pp. 184-208 (2015)

[110] Mani, A., Larsson, J. & Moin, P. Suitability of artificial bulk viscosity for large-eddy simulation of turbulent flows with shocks. *Journal Of Computational Physics*. **228**, 7368-7374 (2009)

[111] Bhagatwala, A., Larsson, J. & Lele, S. A modified artificial viscosity approach for compressible turbulence simulations. *APS Division Of Fluid Dynamics Meeting Abstracts*. **61** pp. AC-001 (2008)

[112] Tadmor, E. Convergence of spectral methods for nonlinear conservation laws. *SIAM Journal On Numerical Analysis*. **26**, 30-44 (1989)

[113] Guo, B., Ma, H. & Tadmor, E. Spectral vanishing viscosity method for nonlinear conservation laws. *SIAM Journal On Numerical Analysis*. **39**, 1254-1268 (2001)

[114] Ghaisas, N., Subramaniam, A. & Lele, S. A unified high-order Eulerian method for continuum simulations of fluid flow and of elastic–plastic deformations in solids. *Journal Of Computational Physics*. **371** pp. 452-482 (2018)

[115] Fiorina, B. & Lele, S. An artificial nonlinear diffusivity method for supersonic reacting flows with shocks. *Journal Of Computational Physics*. **222**, 246-264 (2007)

[116] Johnsen, E., Larsson, J., Bhagatwala, A., Cabot, W., Moin, P., Olson, B., Rawat, P., Shankar, S., Sjögreen, B., Yee, H. & Others Assessment of high-resolution methods for numerical simulations of compressible turbulence with shock waves. *Journal Of Computational Physics*. **229**, 1213-1237 (2010)

[117] Goc, K., Lehmkuhl, O., Park, G., Bose, S. & Moin, P. Large eddy simulation of aircraft at affordable cost: a milestone in computational fluid dynamics. *Flow*. **1** (2021)

[118] Ghate, A., Housman, J., Stich, G., Kenway, G. & Kiris, C. Scale resolving simulations of the NASA Juncture Flow Model using the LAVA solver. *AIAA Aviation 2020 Forum*. pp. 2735 (2020)

[119] Iyer, P. & Malik, M. Wall-modeled LES of the NASA juncture flow experiment. *AIAA Scitech 2020 Forum*. pp. 1307 (2020)

[120] Hendrickson, T., Kartha, A. & Candler, G. An improved Ducros sensor for the simulation of compressible flows with shocks. *2018 Fluid Dynamics Conference*. pp. 3710 (2018)

[121] Ducros, F., Ferrand, V., Nicoud, F., Weber, C., Darracq, D., Gacherieu, C. & Poinsot, T. Large-eddy simulation of the shock/turbulence interaction. *Journal Of Computational Physics*. **152**, 517-549 (1999)

[122] Hill, D. & Pullin, D. Hybrid tuned center-difference-WENO method for large eddy simulations in the presence of strong shocks. *Journal Of Computational Physics*. **194**, 435-450 (2004)

[123] Visbal, M. & Gaitonde, D. Shock capturing using compact-differencing-based methods. *43rd AIAA Aerospace Sciences Meeting And Exhibit*. pp. 1265 (2005)

[124] Shur, M., Spalart, P., Strelets, M. & Travin, A. An enhanced version of DES with rapid transition from RANS to LES in separated flows. *Flow, Turbulence And Combustion*. **95**, 709-737 (2015)

[125] Tu, G., Deng, X. & Mao, M. Implementing high-order weighted compact nonlinear scheme

on patched grids with a nonlinear interpolation. *Computers & Fluids*. **77** pp. 181-193 (2013)

[126] Bogey, C. & Bailly, C. Computation of a high Reynolds number jet and its radiated noise using large eddy simulation based on explicit filtering. *Computers & Fluids*. **35**, 1344-1358 (2006)

[127] Simens, M., Jiménez, J., Hoyas, S. & Mizuno, Y. A high-resolution code for turbulent boundary layers. *Journal Of Computational Physics*. **228**, 4218-4231 (2009)

[128] Kennedy, C., Carpenter, M. & Lewis, R. Low-storage, explicit Runge–Kutta schemes for the compressible Navier–Stokes equations. *Applied Numerical Mathematics*. **35**, 177-219 (2000)

[129] Choi, H. & Moin, P. Effects of the computational time step on numerical solutions of turbulent flow. *Journal Of Computational Physics*. **113**, 1-4 (1994)

[130] Bernardini, M. & Pirozzoli, S. A general strategy for the optimization of Runge–Kutta schemes for wave propagation phenomena. *Journal Of Computational Physics*. **228**, 4182-4199 (2009)

[131] Colonius, T. Modeling artificial boundary conditions for compressible flow. *Annu. Rev. Fluid Mech.*. **36** pp. 315-345 (2004)

[132] Poinsot, T. & Lelef, S. Boundary conditions for direct simulations of compressible viscous flows. *Journal Of Computational Physics*. **101**, 104-129 (1992)

[133] Pirozzoli, S. & Colonius, T. Generalized characteristic relaxation boundary conditions for unsteady compressible flow simulations. *Journal Of Computational Physics*. **248** pp. 109-126 (2013)

[134] Wu, X. Inflow turbulence generation methods. *Annual Review Of Fluid Mechanics*. **49** pp. 23-49 (2017)

[135] Lund, T., Wu, X. & Squires, K. Generation of turbulent inflow data for spatially-developing boundary layer simulations. *Journal Of Computational Physics*. **140**, 233-258 (1998)

[136] Xu, S. & Martin, M. Assessment of inflow boundary conditions for compressible turbulent boundary layers. *Physics Of Fluids*. **16**, 2623-2639 (2004)

[137] Tamura, T. Towards practical use of LES in wind engineering. *Journal Of Wind Engineering And Industrial Aerodynamics*. **96**, 1451-1471 (2008)

[138] Tam, C. Recent advances in computational aeroacoustics. *Fluid Dynamics Research*. **38**, 591 (2006)

[139] Sembian, S., Liverts, M., Tillmark, N. & Apazidis, N. Plane shock wave interaction with a cylindrical water column. *Physics Of Fluids*. **28**, 056102 (2016)

[140] Barone, M. & Lele, S. A numerical technique for trailing edge acoustic scattering problems. *40th AIAA Aerospace Sciences Meeting & Exhibit*. pp. 226 (2002)

[141] Arakawa, A. Computational design for long-term numerical integration of the equations of fluid motion: Two-dimensional incompressible flow. Part I. *Journal Of Computational Physics*. **1**, 119-143 (1966)

[142] Kawai, S., Shankar, S. & Lele, S. Assessment of localized artificial diffusivity scheme for large-eddy simulation of compressible turbulent flows. *Journal Of Computational Physics*. **229**, 1739-1762 (2010)

[143] Nagarajan, S., Lele, S. & Ferziger, J. A robust high-order compact method for large eddy simulation. *Journal Of Computational Physics*. **191**, 392-419 (2003)

[144] Bhaskaran, R. & Lele, S. Heat transfer prediction in high pressure turbine cascade with free-stream turbulence using LES. *41st AIAA Fluid Dynamics Conference And Exhibit*. pp. 3266 (2011)

[145] Sharma, A., Bhaskaran, R. & Lele, S. Large-eddy simulation of supersonic, turbulent mixing layers downstream of a splitter plate. *49th AIAA Aerospace Sciences Meeting Including The New Horizons Forum And Aerospace Exposition*. pp. 208 (2011)

[146] Jain, S. & Moin, P. A kinetic energy–and entropy-preserving scheme for the simulation of

compressible two-phase turbulent flows. *Center For Turbulence Research Annual Research Briefs*. pp. 299-312 (2020)

[147] Yalla, G., Oliver, T. & Moser, R. Numerical dispersion effects on the energy cascade in large-eddy simulation. *Physical Review Fluids*. **6**, L092601 (2021)

[148] Vichnevetsky, R. Wave propagation and reflection in irregular grids for hyperbolic equations. *Applied Numerical Mathematics*. **3** pp. 133-166 (1987)

[149] Vichnevetsky, R. Propagation properties of semi-discretizations of hyperbolic equations. *Mathematics And Computers In Simulation*. **22**, 98-102 (1980)

[150] Yalla, G., Oliver, T., Haering, S., Engquist, B. & Moser, R. Effects of resolution inhomogeneity in large-eddy simulation. *Physical Review Fluids*. **6**, 074604 (2021)

[151] Deng, X., Jiang, Y., Mao, M., Liu, H., Li, S. & Tu, G. A family of hybrid cell-edge and cell-node dissipative compact schemes satisfying geometric conservation law. *Computers & Fluids*. **116** pp. 29-45 (2015)

[152] Mattsson, K. & Nordström, J. Summation by parts operators for finite difference approximations of second derivatives. *Journal Of Computational Physics*. **199**, 503-540 (2004)

[153] Fernández, D., Hicken, J. & Zingg, D. Review of summation-by-parts operators with simultaneous approximation terms for the numerical solution of partial differential equations. *Computers & Fluids*. **95** pp. 171-196 (2014)

[154] Yue, P., Feng, J., Liu, C. & Shen, J. A diffuse-interface method for simulating two-phase flows of complex fluids. *Journal Of Fluid Mechanics*. **515** pp. 293-317 (2004)

[155] Jain, S., Mani, A. & Moin, P. A conservative diffuse-interface method for compressible two-phase flows. *Journal Of Computational Physics*. **418** pp. 109606 (2020)

[156] Mittal, R. & Moin, P. Suitability of upwind-biased finite difference schemes for large-eddy simulation of turbulent flows. *AIAA Journal*. **35**, 1415-1417 (1997)

[157] Wong, M. & Lele, S. High-order localized dissipation weighted compact nonlinear scheme for shock-and interface-capturing in compressible flows. *Journal Of Computational Physics*. **339** pp. 179-209 (2017)

[158] Wong, M. & Lele, S. Multiresolution feature detection in adaptive mesh refinement with high-order shock-and interface-capturing scheme. *46th AIAA Fluid Dynamics Conference*. pp. 3810 (2016)

[159] Donzis, D. Shock structure in shock-turbulence interactions. *Physics Of Fluids*. **24**, 126101 (2012)

[160] Nordström, J. & Carpenter, M. Boundary and interface conditions for high-order finite-difference methods applied to the Euler and Navier–Stokes equations. *Journal Of Computational Physics*. **148**, 621-645 (1999)

[161] Gustafsson, B. The convergence rate for difference approximations to general mixed initial-boundary value problems. *SIAM Journal On Numerical Analysis*. **18**, 179-190 (1981)

[162] Kreiss, H. Initial boundary value problems for hyperbolic systems. *Communications On Pure And Applied Mathematics*. **23**, 277-298 (1970)

[163] Osher, S. Systems of difference equations with general homogeneous boundary conditions. *Transactions Of The American Mathematical Society*. **137** pp. 177-201 (1969)

[164] Gustafsson, B., Kreiss, H. & Sundström, A. Stability theory of difference approximations for mixed initial boundary value problems. II. *Mathematics Of Computation*. **26**, 649-686 (1972)

[165] Trefethen, L. Group velocity interpretation of the stability theory of Gustafsson, Kreiss, and Sundström. *Journal Of Computational Physics*. **49**, 199-217 (1983)

[166] Strikwerda, J. Initial boundary value problems for the method of lines. *Journal Of Computational Physics*. **34**, 94-107 (1980)

[167] Carpenter, M., Gottlieb, D. & Abarbanel, S. The stability of numerical boundary treatments

for compact high-order finite-difference schemes. *Journal Of Computational Physics*. **108**, 272-295 (1993)

[168] Carpenter, M., Gottlieb, D. & Abarbanel, S. Time-stable boundary conditions for finite-difference schemes solving hyperbolic systems: methodology and application to high-order compact schemes. *Journal Of Computational Physics*. **111**, 220-236 (1994)

[169] Svärd, M., Carpenter, M. & Nordström, J. A stable high-order finite difference scheme for the compressible Navier–Stokes equations, far-field boundary conditions. *Journal Of Computational Physics*. **225**, 1020-1038 (2007)

[170] Svärd, M. & Nordström, J. A stable high-order finite difference scheme for the compressible Navier–Stokes equations: no-slip wall boundary conditions. *Journal Of Computational Physics*. **227**, 4805-4824 (2008)

[171] Motheau, E., Almgren, A. & Bell, J. Navier–stokes characteristic boundary conditions using ghost cells. *AIAA Journal*. **55**, 3399-3408 (2017)

[172] Tam, C. & Dong, Z. Wall boundary conditions for high-order finite-difference schemes in computational aeroacoustics. *Theoretical And Computational Fluid Dynamics*. **6**, 303-322 (1994)

[173] Berland, J., Bogey, C., Marsden, O. & Bailly, C. High-order, low dispersive and low dissipative explicit schemes for multiple-scale and boundary problems. *Journal Of Computational Physics*. **224**, 637-662 (2007)

[174] Tam, C. & Hu, F. An optimized multi-dimensional interpolation scheme for computational aeroacoustics applications using overset grid. *10th AIAA/CEAS Aeroacoustics Conference*. pp. 2812 (2004)

[175] Bhaskaran, R. Large eddy simulation of high pressure turbine cascade. (Stanford University, 2010)

[176] Song, H., Matsuno, K., West, J., Subramaniam, A., Ghate, A. & Lele, S. Scalable Parallel Linear Solver for Compact Banded Systems on Heterogeneous Architectures. *Journal Of Computational Physics*. pp. 111443 (2022)

[177] Davidson, A., Zhang, Y. & Owens, J. An auto-tuned method for solving large tridiagonal systems on the GPU. *2011 IEEE International Parallel & Distributed Processing Symposium*. pp. 956-965 (2011)

[178] Kim, H., Wu, S., Chang, L. & Wen-mei, W. A scalable tridiagonal solver for GPUs. *2011 International Conference On Parallel Processing*. pp. 444-453 (2011)

[179] Tian, Y., Jaberi, F., Li, Z. & Livescu, D. Numerical study of variable density turbulence interaction with a normal shock wave. *Journal Of Fluid Mechanics*. **829** pp. 551-588 (2017)

[180] Liu, X., Zhang, S., Zhang, H. & Shu, C. A new class of central compact schemes with spectral-like resolution I: Linear schemes. *Journal Of Computational Physics*. **248** pp. 235-256 (2013)

[181] Ffowcs Williams, J. & Hawkings, D. Sound generation by turbulence and surfaces in arbitrary motion. *Philosophical Transactions Of The Royal Society Of London. Series A, Mathematical And Physical Sciences*. **264**, 321-342 (1969)

[182] Lockard, D. An efficient, two-dimensional implementation of the Ffowcs Williams and Hawkings equation. *Journal Of Sound And Vibration*. **229**, 897-911 (2000)

[183] Spalart, P. & Shur, M. Variants of the Ffowcs Williams-Hawkings equation and their coupling with simulations of hot jets. *International Journal Of Aeroacoustics*. **8**, 477-491 (2009)